Uncovering clinically-relevant altered antibiotic responses of *Staphylococcus aureus* under wound infection-mimetic conditions

Colin D. Rieger[1], Ali Molaeitabari[1], Tanya E. S. Dahms[1] and Omar M. El-Halfawy[1*]

[1] Department of Chemistry and Biochemistry, Faculty of Science, University of Regina, Regina, SK, S4S 0A2, Canada

[*] Correspondence: omar.el-halfawy@uregina.ca (O.M.E.)

Running title: Altered antibiotic responses of *S. aureus* under wound-like conditions

Abstract:

Chronic wound infections, most commonly caused by *Staphylococcus aureus*, affect 1-2% of the world's population and incur direct healthcare costs exceeding $300B per year. Bacterial susceptibility to antibiotics is typically determined by standard *in vitro* antimicrobial susceptibility testing (AST) using Mueller-Hinton broth (MHB). However, the results from these assays often do not correlate with therapeutic outcomes, potentially because the test conditions do not reflect those at the infection site. We sought to determine the antibiotic susceptibility of methicillin-resistant *S. aureus* (MRSA) in simulated wound fluid (SWF), a medium resembling wound exudate, compared with MHB. We observed discordance in AST results for representative antibiotics across six of nine antibiotic classes tested in SWF compared with MHB against MRSA USA300. The antibiotic classes showing the most significant discordant AST results included tetracyclines, to which USA300 was more resistant (up to a 128-fold shift), and β-lactams, to which MRSA was unexpectedly more sensitive (up to a 256-fold shift) when tested in SWF. Genome-wide assays and subsequent mechanistic characterizations revealed that the increased resistance to tetracyclines is mediated by MntC, an extracellular binding protein of a manganese ABC transporter system, whereas the drastic sensitization to β-lactams was driven by cell envelope remodelling in SWF. Further, *Galleria mellonella* incision wound infection results matched the *in* vitro susceptibility phenotypes of the tetracycline doxycycline and the β-lactam cefuroxime in SWF but not in MHB, suggesting that this host-mimetic medium is a better predictor of MRSA *in vivo* wound infection therapeutic outcomes. Together, this work addresses the relatively long-recognized shortcomings of the MHB-based standard AST by uncovering alterations in MRSA antibiotic susceptibility in wound exudate-like fluid relative to MHB. It uncovers potentially clinically relevant antibiotic response determinants, identifying MntC as a

36 potential new target for adjuvant therapy. Our results may also guide improved antibiotic

37 therapeutic choices for drug-resistant MRSA wound infections.

38

39 **Introduction**

40 Antibiotic resistance is rising at an alarming rate, and existing antibiotics are failing to
41 treat infections (1). This crisis further complicates chronic infections, which pose significant
42 healthcare and socioeconomic challenges (2). Chronic wounds are particularly troublesome
43 because they have a prolonged inflammatory phase and delayed healing, leading to tissue fibrosis
44 and non-healing ulcers (3, 4). Wound exudates produced during healing are serum-based fluid
45 rich in protein and growth factors, providing a suitable environment for bacterial colonization
46 (5); such infections frequently fail to respond to treatment (3). Chronic wound infections are
47 estimated to affect 1-2% of the world population at some point in their lives (6). Wound care
48 poses a substantial economic burden on the healthcare system; wound care costs were estimated
49 to be ~$300B worldwide in 2019 (7) – such expenditures in the 10 highest spending countries
50 alone increased from ~$233B in 2019 to $301B in 2022 (8).

51 *Staphylococcus aureus,* a Gram-positive pathogen, is a leading cause of both hospital-
52 and community-acquired infections worldwide, associated with bacteremia, endocarditis, skin
53 and soft tissue infections (SSTIs), and other infections affecting almost all body sites (9-11).
54 Notably, *S. aureus* is the leading cause of SSTIs, including complicated SSTIs such as chronic
55 wounds and burn infections **(11-13)**. If not treated, *S. aureus* wound infections can spread to
56 bloodstream infections, which are often fatal **(14)**. *S. aureus* developed multi-drug resistance,
57 including to last-resort antibiotics, placing it on the World Health Organization's list of 'priority
58 pathogens' posing the greatest threat to human health (15). Methicillin-resistant *S. aureus*
59 (MRSA, known for resistance to β-lactam antibiotics) is the leading cause of wound infections,
60 posing severe clinical problems (13). Currently, the most commonly circulating community-
61 associated MRSA lineage in North America is USA300 **(16)**. The discovery of new antibiotics

62 has lagged behind the constant rise in AMR prevalence **(10)**. There is an urgent need for new
63 antimicrobial solutions, including antibiotic adjuvants that revive currently failing antibiotics.
64 Bacterial antibiotic responses are often studied under standard *in vitro* conditions [e.g.,
65 Mueller-Hinton broth (MHB), composed of beef extract, casein hydrolysate, and starch(17)] that
66 do not adequately reflect the infection site. These assays, standardized by agencies such as
67 CLSI(18), are routinely used in clinical labs worldwide to determine whether a clinical isolate is
68 sensitive or resistant to an antibiotic, guiding antibiotic therapy. Nonetheless, the clinical
69 outcome often does not correlate with standard antibiotic susceptibility test (AST) results, with
70 reports of unexpected antibiotic therapeutic failure (19-21). In contrast, unexpected potency in
71 patients despite AST-predicted resistance is far less frequently reported, as such antibiotics would
72 typically be contraindicated. However, anecdotal reports describe instances in which an
73 antibiotic empirically prescribed while waiting (up to 72 h) for AST results shows efficacy in
74 patients before AST identifies the causative isolate as resistant to the same antibiotic. Together,
75 standard AST erroneous predictions can lead to therapeutic failure or sideline much-needed *in*
76 *vivo*-effective antibiotics.
77 Culture conditions and media composition dictate gene expression and dispensability
78 profiles in bacteria to meet their survival requirements (22, 23), thereby potentially altering
79 bacterial antibiotic responses. Infection-mimetic media, such as simulated wound fluid (SWF)
80 (24), have been developed, providing test conditions that are more clinically relevant than MHB
81 for assessing bacterial responses. SWF is composed of 50% v/v fetal bovine serum in maximal
82 recovery diluent, which is an isotonic peptone saline solution (24). Such a formulation of SWF
83 mimics chronic wound exudates, as the latter are derived from serum and contain electrolytes at
84 concentrations equivalent to those in serum, approximately half the total protein content of

85 serum, and higher levels of growth factors for tissue regeneration (25-29). The inclusion of fetal
86 bovine serum in this recipe provides additional components not present in MHB, such as growth
87 factors, transport proteins, enzymes, hormones, fatty acids, and lipids, at biologically relevant
88 levels (30, 31).

89 Here, we used SWF to evaluate the antimicrobial susceptibility profile of MRSA under
90 wound infection-mimetic conditions. We observed discordance in AST results for representative
91 antibiotics across six of nine antibiotic classes tested in SWF compared to MHB against the
92 MRSA USA300. The antibiotic classes showing the most significant discordant AST results
93 included tetracyclines, to which USA300 was more resistant (up to a 128-fold shift), and β-
94 lactams, to which the MRSA was unexpectedly more sensitive (up to a 256-fold shift), when
95 tested in SWF. Interestingly, these antibiotic susceptibility shifts crossed the CLSI clinical
96 breakpoint for representatives of both classes, suggesting they may result in altered therapeutic
97 outcomes. Genome-wide assays and subsequent mechanistic characterizations revealed that the
98 increased resistance to tetracyclines is mediated by MntC, an extracellular binding protein of a
99 manganese ABC transporter system, whereas the drastic sensitization to β-lactams was driven by
100 cell envelope remodelling in SWF. Further, we used a *Galleria mellonella* incision wound
101 infection model, which shows wound healing events similar to those in animals (32) and
102 recapitulates the hallmarks of trauma and infection observed in mammalian models (33), to
103 characterize the observed *in vitro* phenotypes. Doxycycline, a tetracycline antibiotic, could not
104 rescue wild-type USA300-infected Galleria larvae but significantly increased the survival of
105 those infected with the *mntC*::Tn mutant, whereas the β-lactam cefuroxime was effective at
106 rescuing a significant number of USA300-infected larvae. These *in vivo* results matched the *in*

107 *vitro* phenotypes in SWF but not MHB, suggesting that this host-mimetic medium is a better
108 predictor of *in vivo* MRSA wound infection therapeutic outcomes.
109 Together, this work addresses the relatively long-recognized shortcomings of the MHB-
110 based standard AST by uncovering alterations in MRSA antibiotic susceptibility in wound
111 exudate-like fluid relative to MHB. By studying the mechanisms underlying discordant results
112 between standard and infection-mimetic conditions at the whole-genome level, we uncovered
113 potentially clinically relevant antibiotic response determinants. Our results may guide improved
114 antibiotic selection in the clinic and provide a potential new target for adjuvant therapy against
115 drug-resistant MRSA wound infections.
116
117 **Results:**
118 **Alterations in MRSA sensitivity to antibiotics in SWF.**
119 We first compared AST results of representative antibiotics from nine classes against
120 USA300 cultured in MHB and SWF (Table 1). Six of the nine classes showed discordance in
121 minimum inhibitory concentration (MIC) determined in the two media (MIC ≥ 4-fold difference
122 between SWF and MHB, Table 1). The antibiotic classes showing the most significant fold shift
123 in MIC in SWF relative to MHB included tetracyclines that showed an increase in MIC when
124 tested in SWF (e.g., a 128-fold shift for tetracycline) and β-lactams that showed a decrease in
125 MIC in SWF (e.g., a 256-fold shift for cefuroxime, Table 1). Importantly, the MIC fold shifts
126 crossed the CLSI clinical breakpoint for representatives of these two classes (Table 1). Together,
127 we chose to focus on these classes to uncover the mechanism underlying the observed altered
128 antibiotic susceptibility under the wound-mimetic condition.

129 Tetracycline antibiotics inhibit protein synthesis by binding to the 30S ribosome subunit
130 (34). Doxycycline is a second-generation tetracycline that showed a 32-fold increase in MIC
131 against USA300 in SWF (Table 1). In addition, we assessed the third-generation tetracycline,
132 omadacycline, and found that its MIC against USA300 doubled in SWF relative to MHB (Table
133 1). These results demonstrate that the increased resistance in SWF is conserved across the three
134 generations of tetracyclines. Doxycycline is more clinically relevant than tetracycline for treating
135 MRSA skin and soft tissue infections (SSTIs) **(35)**; therefore, we used it as a representative of
136 this class in the remainder of this study. On the other hand, cefuroxime is a β-lactam antibiotic
137 that binds to penicillin-binding protein 2, inhibiting bacterial cell wall synthesis (36). Oxacillin,
138 another β-lactam, is used by CLSI to distinguish MRSA from methicillin-sensitive *S. aureus*
139 (MSSA) **(18)**; it showed a 64-fold decrease in MIC against USA300 in SWF, bringing the MIC
140 below the CLSI MRSA breakpoint (Table 1). We initially tested both β-lactams and then focused
141 on cefuroxime for subsequent mechanistic testing.
142 To determine how conserved the doxycycline and β-lactam susceptibility alterations in
143 SWF are across multiple MRSA strains, we determined the MICs of antibiotics against a panel of
144 isolates representing the most commonly circulating lineages of MRSA in Canada [CMRSA
145 strains **(37)**] in both MHB and SWF. All CMRSA strains showed increased resistance (≥ 8-fold
146 shift in MIC) to doxycycline when tested in SWF relative to MHB (Table 2). All CMRSA strains
147 exhibited increased sensitivity to both β-lactams in SWF, except for CMRSA 1 and CMRSA 4,
148 with MIC shifts in CMRSA 5, 7, 8, and 10 crossing the CLSI breakpoint for one or both
149 antibiotics (Table 2). Given the magnitude of antibiotic susceptibility alterations conserved
150 across strains from multiple MRSA lineages, we next sought to determine the mechanisms of
151 doxycycline and cefuroxime susceptibility alterations in the wound-mimetic medium in MRSA

152 using USA300 as a representative being one of the most common community-associated MRSA

153 strains.

154 **Table 1. USA300 MIC assays conducted in SWF relative to those in MHB**

155 MICs from at least three independent experiments.

Antibiotic class	Antibiotic	MIC, µg/mL		Fold	CLSI breakpoint, µg/mL		
		MHB	SWF	shift*	R, ≥	S, ≤	Ref
Lipopeptides	Daptomycin	4	1	4 ↓	-	1	(38)
Fluoroquinolones	Ciprofloxacin	32	16	2 ↓	4	1	(38)
Glycopeptides	Vancomycin	2	1	2 ↓	16	2	(38)
Rifampins	Rifampicin	0.008	0.064	8 ↑	4	1	(38)
β-lactams	Cefuroxime	1024	4	256 ↓	32	8	(39)
	Oxacillin	64	1	64 ↓	4	2	(38)
Polymyxins	Colistin	512	32	16 ↓			
Tetracyclines	Tetracycline	0.25	32	128 ↑	16	4	(38)
	Doxycycline	0.125	4	32 ↑	16	4	(38)
	Omadacycline	0.25	0.5	2 ↑			
Macrolides	Azithromycin	2	0.0156	128 ↓	8	2	(38)
Aminoglycosides	Kanamycin	4	4	No shift	64	16	(18)

156 * Fold increase or decrease in SWF relative to MHB.

157

158 **Table 2. MIC of cefuroxime, oxacillin, and doxycycline against isolates representing the**

159 **most commonly circulating lineages of MRSA in Canada.** MICs average of three independent

160 experiments.

Strain	Lineage	MIC in MHB (µg/mL)			MIC in SWF (µg/mL)		
		cefuroxime	oxacillin	doxycycline	cefuroxime	oxacillin	doxycycline
CMRSA 1	USA600	>2048	1024	0.25	>2048	1024	2
CMRSA 2	USA100/800	>2048	512	0.25	16	32	4
CMRSA 3		>2048	512	16	512	256	>128
CMRSA 4	USA200	2048	256	0.25	2048	256	4
CMRSA 5	USA500	256	32	8	8	1	>128
CMRSA 6		>2048	512	16	1024	256	>128
CMRSA 7	USA400/MW2	1024	64	0.25	8	2	2
CMRSA 8	EMRSA15	1024	64	0.25	4	8	2
CMRSA 9		2048	256	0.25	16	32	4
CMRSA 10	USA300	1024	64	0.25	4	2	4

161

162 **A chemogenomic screen to uncover the mechanism of increased resistance to doxycycline in**

163 **SWF.**

164 To investigate the increased resistance of USA300 to doxycycline when cultured in SWF,
165 we screened the Nebraska Transposon Mutant Library (NTML), a sequence-defined transposon
166 insertion library comprising 1920 mutants that cover the non-essential genome of USA300 **(40)**,
167 at supra-inhibitory (in MHB) and sub-inhibitory (in SWF) concentrations of doxycycline. The
168 NTML supra-inhibitory screen in MHB (at 1 µg/mL doxycycline, 8X the MIC in MHB), which
169 aimed to identify putative sensitivity determinants, and follow-up dose-response assays did not
170 reveal any mutants more resistant to doxycycline in MHB relative to the wild-type
171 (Supplementary Fig. 1A-C). On the other hand, the NTML sub-inhibitory screen in SWF (at
172 0.125 µg/mL doxycycline, 1/32nd the MIC in SWF), which aimed to identify putative
173 determinants of doxycycline resistance, and follow-up MIC assays revealed that *mntB*::Tn and
174 *mntC*::Tn were sensitive to doxycycline in SWF relative to USA300 (Fig. 1A-C and
175 Supplementary Fig. 2). To verify the observed phenotypes, we genetically complemented *mntB*
176 and *mntC* in their transposon mutants. While *mntC* complementation restored doxycycline
177 resistance of *mntC*::Tn, *mntB* alone was not sufficient to restore doxycycline resistance in
178 *mntB*::Tn, but rather both *mntB* and *mntC* were required (Supplementary Fig. 3A-C). As such,
179 the *mntB*::Tn phenotype may be due to polar effects from the transposon insertion into *mntB,*
180 disrupting the downstream *mntC* (Supplementary Fig. 3C). Together, this work identifies MntC
181 as the determinant of increased doxycycline resistance in the wound-like medium.

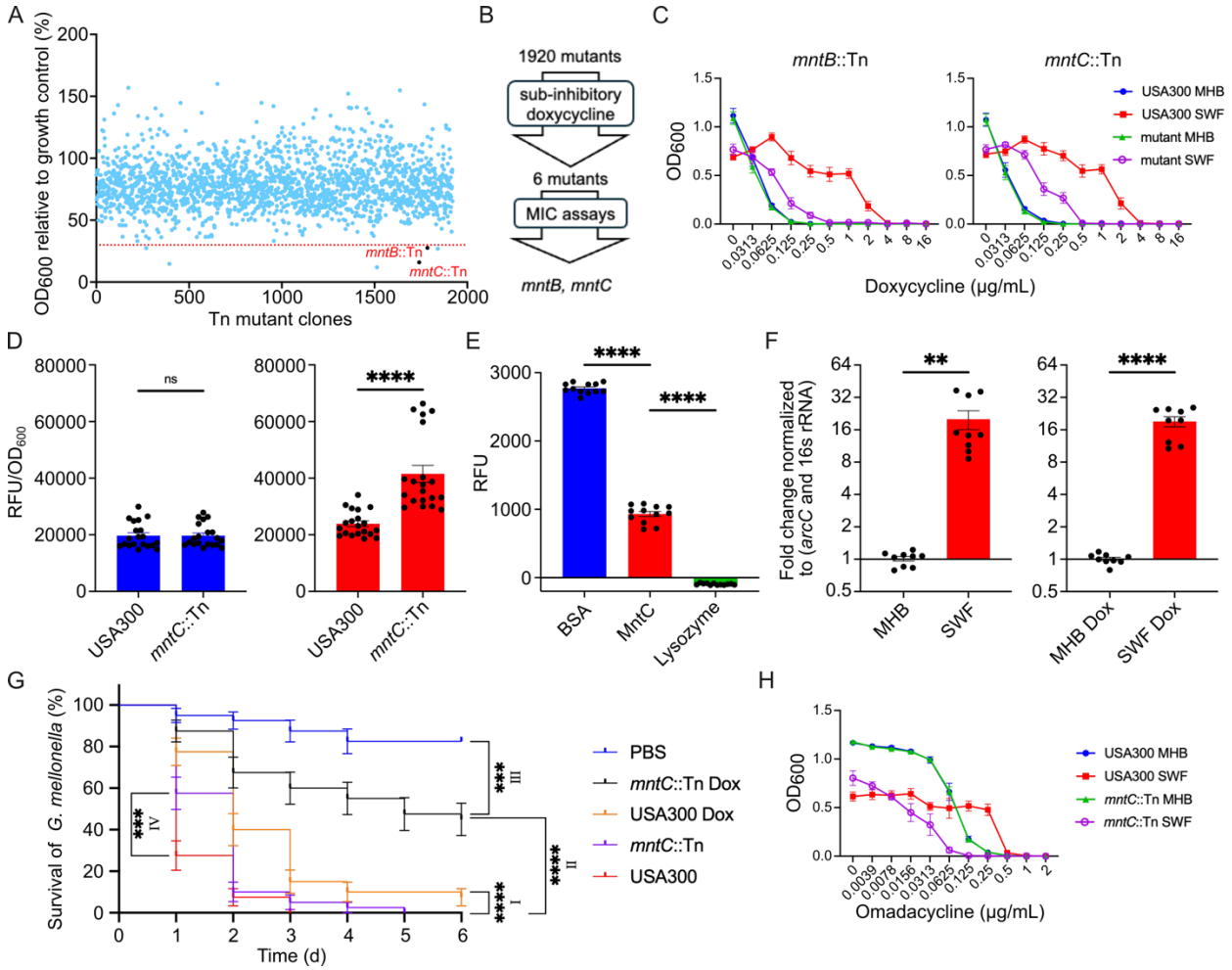

Fig. 1 | MntC increases USA300 resistance to doxycycline in SWF

A) A chemogenomic screen of the Nebraska Transposon Mutant Library with doxycycline at 1/32th the MIC in SWF. B) Workflow of the chemogenomic screen and follow-up assays that lead to the putative determinants of doxycycline resistance. C) MIC assays of determinants of USA300 doxycycline resistance in SWF. n = 9 from three independent experiments, shown as mean ± SEM. D) Intracellular fluorescence of doxycycline relative fluorescent units (RLU)/OD_{600} in USA300 and *mntC*::Tn cultured in MHB (blue) or SWF (red). n = 20 from 4 independent experiments. E) Doxycycline binding assay showing increased RFU upon doxycycline binding with the ligands bovine serum albumin (positive control), MntC, and lysozyme (negative control). n = 12. F) Fold change in *mntC* transcription from USA300 in SWF

193 and MHB with or without doxycycline (relative to averaged signals in MHB). n = 9 from three
194 independent experiments. G) Kaplan-Meier survival curve of *G. mellonella* treated with
195 doxycycline or vehicle control, shown as mean ± SE. n = 40 from 4 independent experiments.
196 H) MIC assays of omadacycline against USA300 and *mntC*::Tn cultured in SWF and MHB. n =
197 6 from three independent experiments, shown as mean ± SEM. Significant difference were
198 determined between USA300 cultured in MHB and SWF for D, E, F by Welch's t-test, and in G
199 (I; USA300 and USA300 Dox), (II; *mntC*::Tn and *mntC*::Tn Dox) and (III; *mntC*::Tn Dox and
200 PBS) by Logrank (Mantel-Cox) test and (IV; *mntC*::Tn and USA300) at day 1 by two-way
201 ANOVA and the Tukey post hoc test. $p < 0.0001$ (****), $p < 0.001$ (***), $p < 0.01$ (**), $p < 0.05$
202 (*).
203
204 **MntC increases doxycycline resistance in wound-like medium.**
205 Next, we set out to determine the mechanism by which MntC increases doxycycline
206 resistance in SWF. MntABC, an ABC transporter that imports manganese, is comprised of an
207 ATP-binding protein (MntA), a transmembrane protein (MntB), and an extracellular binding
208 protein (MntC) **(41);** therefore, we initially hypothesized that manganese or other divalent
209 cations imported by MntC contributed to the increased resistance to doxycycline. However,
210 exogenously supplementing manganese, calcium, magnesium, cobalt, iron, copper, and zinc, in
211 dose-dependent checkerboard assays with doxycycline against wild-type USA300 and *mntC*::Tn
212 in MHB did not alter the susceptibility to doxycycline except for iron, which showed antagonism
213 in both strains suggesting the observed iron effect is MntC-independent (Supplementary Fig. 4).
214 Conversely, higher concentrations of manganese antagonized doxycycline in SWF both in the
215 wild-type and the *mntC* mutant (FICI = 6.75 and 32.5, respectively; Supplementary Fig. 5). Such

216 effect might be due to compensation of the sequestration of manganese in SWF due to chelators,
217 such as calprotectin, likely present in fetal bovine serum. Together, manganese and other divalent
218 cations appear to play no role in the MntC-mediated doxycycline resistance observed in SWF.
219 Next, we hypothesized that MntC sequesters doxycycline, lowering its intracellular
220 concentration, thereby increasing resistance to that antibiotic in bacteria cultured in SWF. To
221 address this hypothesis, we first determined the intracellular concentration of doxycycline in
222 *mntC*::Tn relative to the wild-type cultured in MHB and SWF. In SWF, *mntC*::Tn had a greater
223 intracellular concentration of doxycycline relative to USA300, whereas both the wild-type and
224 mutant strains showed similar intracellular doxycycline content in MHB (Fig. 1D), aligning with
225 our previous results showing a SWF-specific role of MntC in doxycycline resistance and
226 supporting our hypothesis of a potential sequestration of doxycycline by MntC. Next, we
227 assessed the ability of purified recombinant MntC to bind doxycycline using a fluorescent
228 binding assay in which doxycycline fluorescence increased upon binding to a ligand. Using
229 bovine serum albumin and lysozyme as positive **(42)** and negative controls, respectively, in this
230 assay, we revealed that MntC binds doxycycline (Fig. 1E), which likely reduces its intracellular
231 concentration (Fig. 1D). Given that such a binding interaction does not require any component of
232 SWF, as it occurred in HEPES buffer, we posited that MntC-mediated increased doxycycline
233 resistance occurs in SWF only due to an upregulation of *mntC* under wound-like conditions.
234 Hence, we assessed the transcriptional differences in *mntC* using qRT-PCR. We revealed that
235 *mntC* was upregulated by ~20-fold in wild-type USA300 cultured in SWF relative to MHB,
236 irrespective of doxycycline treatment (Fig. 1F), demonstrating that the *mntC* upregulation is
237 induced by the wound-like culture condition rather than a specific response to doxycycline. In
238 fact, doxycycline exposure downregulated *mntC* in USA300 in both SWF and MHB to a similar

239 extent (~4-fold; Supplementary Fig. 6). In summary, the increase in doxycycline resistance in the
240 wound-like medium is due to an upregulation of *mntC*, whereby the overexpressed MntC can
241 sequester doxycycline, decreasing its effective intracellular concentration.
242
243 **MntC contributes to doxycycline resistance *in vivo* in a *Galleria mellonella* wound infection**
244 **model.**
245 Next, we sought to assess whether MntC contributed to doxycycline resistance in vivo in
246 a wound infection model. To that end, we tested the *mntC*::Tn mutant in a *Galleria mellonella*
247 incision wound infection model. Galleria mounts both cellular and humoral innate immune
248 responses closely resembling those of vertebrates and thrives at mammalian body temperature
249 (43, 44). Incision wounds have been histologically characterized in Galleria larvae, showing
250 wound healing events similar to those in animals (32), and their wound model recapitulates the
251 hallmarks of trauma and infection observed in mammalian models (33). Infection with either the
252 wild-type USA300 or the *mntC*::Tn mutant, both treated with the vehicle control (Glaxal™ Base
253 non-medicated cream), led to 100% larval fatality by the end of the experiment (at 6 days);
254 however, we observed a significant increase in survival of larvae infected with *mntC*::Tn relative
255 to USA300 at day 1 (Fig. 1G), suggesting a role of MntC in virulence. Further, a single dose of
256 doxycycline treatment (4 μL of 10% w/w cream, i.e., 0.4 mg/incision) increased survival of
257 *mntC*::Tn-infected larvae to 45% compared to only 7.5% survival in wild-type-infected ones
258 (Fig. 1G). Together, knocking out *mntC* increased the sensitivity of USA300 to doxycycline *in*
259 *vivo,* consistent with the *in vitro* SWF phenotype, demonstrating that MntC is a potential target
260 for doxycycline adjuvant therapy for MRSA wound infections.
261

262 **A chemogenomic screen to uncover the mechanism of MRSA susceptibility to β-lactams in**
263 **SWF.**

264 To investigate the increased sensitivity of USA300 to cefuroxime in SWF, we screened
265 the NTML in SWF at 16 µg/mL of cefuroxime (4X the wild-type MIC in SWF) to identify
266 susceptibility determinants. However, none of the mutants with greater than 25% relative growth
267 at this supra-inhibitory concentration in SWF showed increased cefuroxime MIC in follow-up
268 MIC assays (Supplementary Fig. 7A-C). We also screened the NTML in MHB at 128 µg/mL of
269 cefuroxime (1/8th the wild-type MIC in MHB) to identify putative determinants of cefuroxime
270 resistance, revealing 101 mutants with <8% growth at this sub-inhibitory concentration relative
271 to their untreated controls (Fig. 2A-B). We hypothesized that mutants of determinants underlying
272 cefuroxime sensitivity in SWF would be susceptible to cefuroxime in MHB, with no further
273 sensitization in SWF relative to the parent strain. To that end, we tested the 101 mutants in dose-
274 response and MIC assays. Nine mutants showed ~128 to 256-fold sensitization to cefuroxime
275 relative to the parent strain in MHB (i.e., showing MICs similar to or within 2-fold of that of
276 USA300 in SWF) with relatively minimal MIC reduction relative to USA300 (≤4-fold) in SWF,
277 revealing putative primary determinants of this phenotype (Fig. 2C). An additional 12 mutants
278 showed a relatively more modest shift in cefuroxime MIC in MHB, potentially identifying
279 secondary determinants of the phenotype (Supplementary Fig. 8).

280 Six of the primary determinants (Fig. 2C) are localized to or involved in cell envelope
281 homeostasis; their gene products are related to peptidoglycan synthesis [*pbp2a* and *pbp4*,
282 encoding penicillin binding proteins (PBPs)], wall teichoic acid [WTA; *tcaA* and *fmtA*], and cell
283 envelope stress response [*graR* and *vraF,* encoding members of the GraXSR-VraFG five-
284 component response system] (45-49). Interestingly, some of the secondary determinants

285 (Supplementary Fig. 8) are involved in similar processes [MurA2, predicted to be involved in
286 biosynthesis and degradation of peptidoglycan; RsbU and RsbV, involved in the regulatory
287 cascade of the master transcriptional regulator σ^B that provides protection from stress and
288 influences cell envelope composition (50)] or localize at the membrane [SAUSA300_2297,
289 SAUSA300_0073, SAUSA300_1785, SAUSA300_1484, SAUSA300_2315, and SpsA;
290 predictions from (51)]. The genes encoding the remaining three primary determinants are
291 SAUSA300_0794 (encodes a TOPRIM domain-containing protein previously shown to be
292 hypersensitive to the β-lactam amoxicillin **(52)**), *aapA* (encodes a D-serine/D-alanine/glycine
293 transporter), and *yabJ* (encodes a putative endo-RNase L-PSP). Importantly, most of the primary
294 cell envelope-related determinants (Fig. 2C) are genetically interconnected as shown in synthetic
295 lethal interaction analyses (53). Given that most mutants identified above harbour disruptions
296 related to the cell envelope, which also comprises the β-lactam target (peptidoglycan), we then
297 set out to characterize the primary cell envelope-related determinants and assess their
298 implications for the unexpected β-lactam hypersensitivity of the MRSA USA300 in the wound-
299 like medium.
300

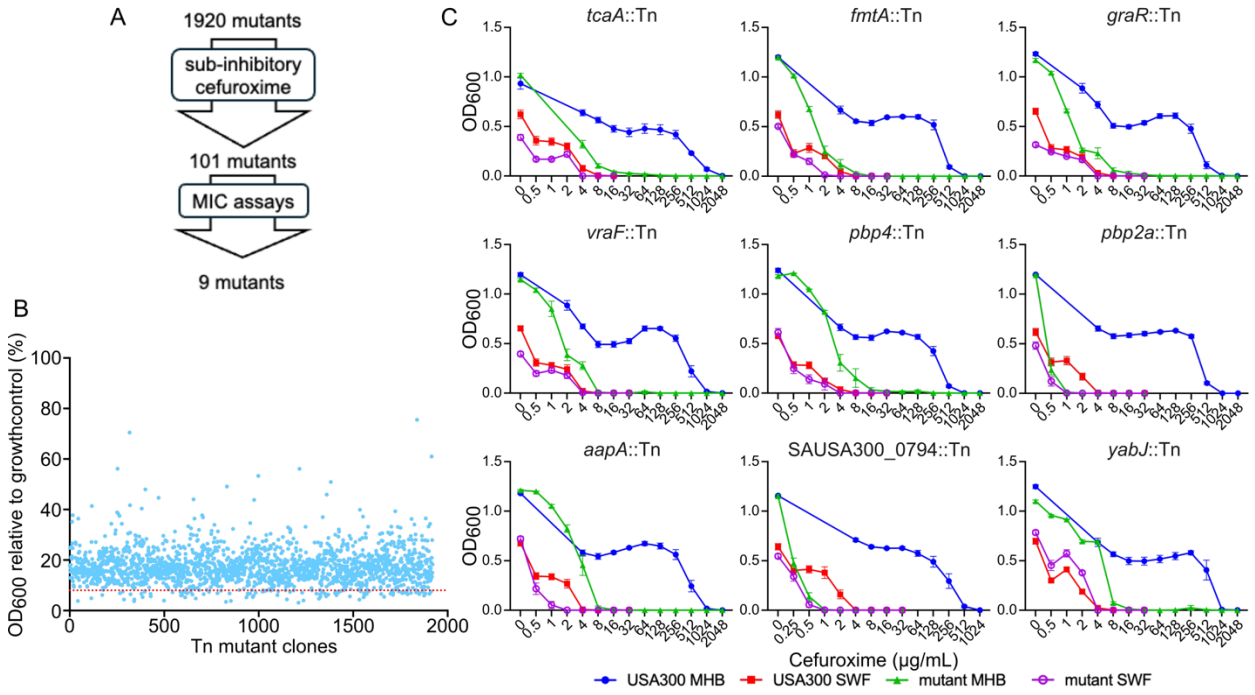

Fig. 2 | A chemogenomic screen identifies putative determinants of USA300 sensitivity to cefuroxime in SWF.

A) The workflow of the chemogenomic screen and follow-up assays that led to the identification of putative determinants of cefuroxime sensitivity. B) A chemogenomic screen of the Nebraska Transposon Mutant Library with cefuroxime at 1/8th MIC of the wild-type strain in MHB. C) MIC assays of putative determinants uncovered in the screen; n ≥ 6 from at least three independent experiments shown as mean ± SEM.

Decreased abundance of penicillin-binding proteins (PBPs) contributes to cefuroxime susceptibility in SWF.

First, we investigated the potential role of alterations in PBPs in the SWF-specific cefuroxime susceptibility phenotype, especially given that PBPs are the main targets of β-lactams and that the primary resistance mechanism of MRSA is the low-affinity alternative

315 PBP2a encoded by *pbp2a* or *mecA* (54). Based on *pbp2a*::Tn and *pbp4*::Tn cefuroxime
316 susceptibility phenotypes (Fig. 2C), we hypothesized that USA300 cultured in SWF would have
317 decreased abundance of these PBPs. To directly assess the abundance of PBPs in USA300, we
318 isolated membrane fractions from cultures grown in MHB and SWF and then used a fluorescent
319 penicillin (BOCILLIN™ FL) to bind and detect PBPs resolved on SDS-PAGE. Quantification of
320 band density identified a ~25, ~21, and ~55 percent reduction in the relative abundance of PBP1,
321 2, and 4, respectively, in SWF compared to MHB (Fig. 3A, Supplementary Fig. 9A, B). Notably,
322 PBP1 and PBP2 are essential genes and therefore are not in the NTML (48). Also, BOCILLIN™
323 FL labels all PBPs except PBP2a due to its decreased affinity for penicillin. Therefore, we
324 assessed PBP2a abundance by Western blot using an anti-PBP2a-specific antibody **(55)**,
325 revealing a ~20 percent decrease in the relative abundance of PBP2a in USA300 cultured in
326 SWF relative to MHB (Fig. 3B, Supplementary Fig. 9C, D). Together, the decreased abundance
327 of the four PBPs (1, 2, 2a, and 4) in SWF is likely a major contributor to the decreased β-lactam
328 susceptibility of USA300 under the wound-like condition.
329

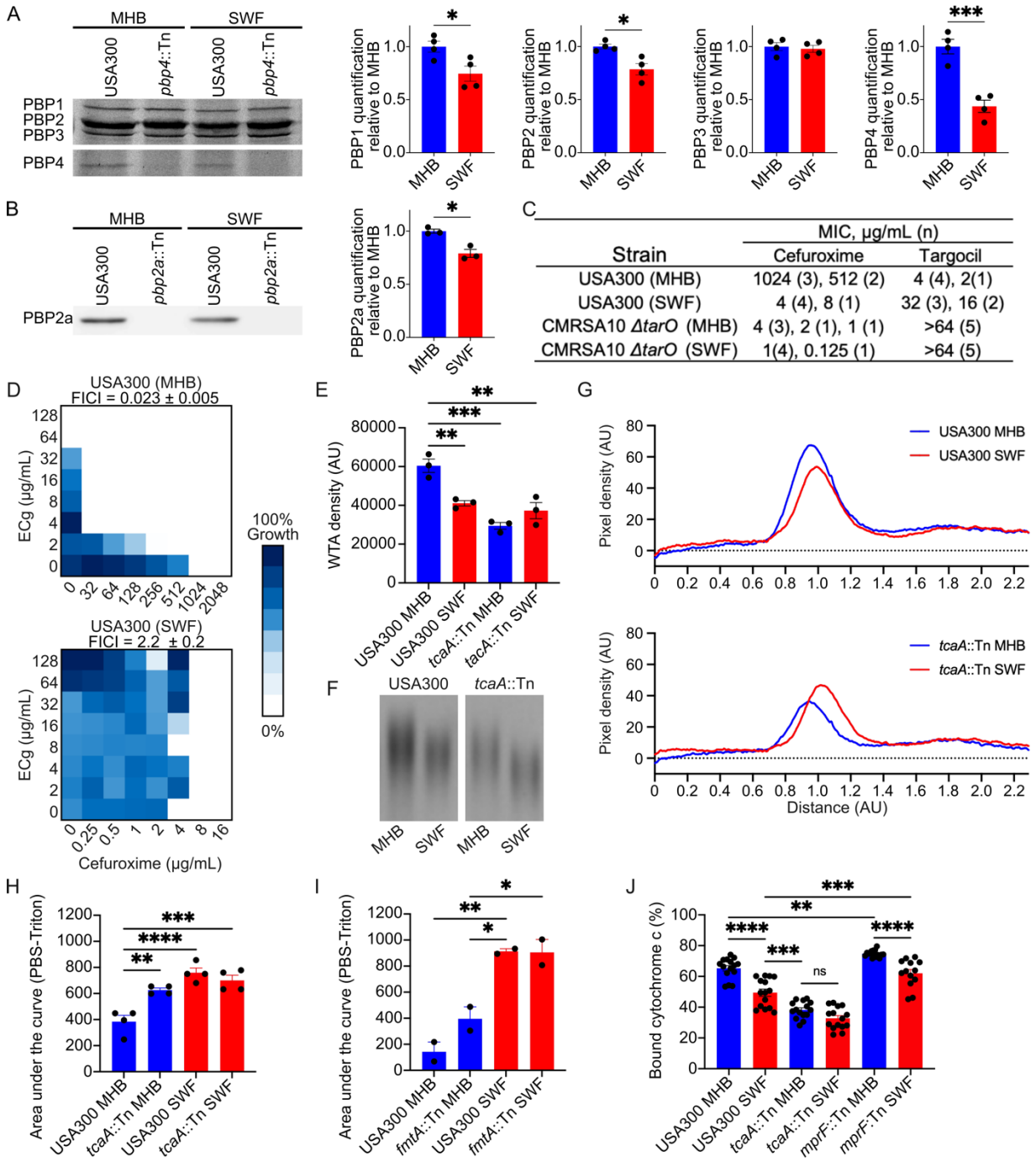

Fig. 3 | Decrease in the abundance of PBPs and wall teichoic acid in SWF contributes to USA300 cefuroxime sensitivity.

A) Quantification of PBP1, 2, 3, 4 from USA300 cultured in SWF (red) relative to MHB (blue), n = 4 from two independent membrane isolations, shown as mean ± SEM and one representative

336 BOCILLIN FL-labeled PBP gel. All uncropped gels are shown in Supplementary Fig. 9. B)
337 PBP2a quantification from Western blots, using an anti-PBP2a antibody, of membranes isolated
338 from USA300 cultured in SWF (red) relative to MHB (blue), n = 3 from three independent
339 membrane isolations, shown as mean ± SEM and one representative blot. All uncropped blots
340 are shown in Supplementary Fig. 9. C) MIC of cefuroxime and targocil against USA300 or
341 CMRSA10*ΔtarO* cultured in MHB or SWF, n = 5 biological replicates each performed in
342 triplicate. D) Representative checkerboard assays of *S. aureus* USA300 of cefuroxime in
343 combination with epicatechin gallate (ECg). n = 5. FICI shown as mean ± SEM. E) Relative
344 quantity of PAGE-resolved crude WTA from *S. aureus* USA300 or *tcaA*::Tn cultured in MHB or
345 SWF. n = 3 shown as mean ± SEM. F) Representative PAGE gel of WTA isolated from USA300
346 or *tcaA*::Tn cultured in MHB or SWF. Uncropped gel is shown in Supplementary Fig. 10. G)
347 Relative band migration of WTA on PAGE represented as mean pixel density. n = 3 from three
348 independent WTA isolations. H-I) Area under the curve (AUC) of lysis rates represented as PBS
349 AUC – 0.02% Triton AUC comparing lysis rates of USA300 and *tcaA*::Tn (H; n=4) and *fmtA*::Tn
350 (I; n=2) cultured from MHB or SWF. Shown as mean ± SEM. Full lysis curves and AUC
351 calculation are shown in Supplementary Fig. 10. J) Percent cytochrome c binding to USA300 or
352 mutants cultured in MHB or SWF, which infers relative cell charge. n = 15 or n = 13 for
353 *mprF*::Tn SWF from 5 independent experiments, shown as mean ± SEM. Significant differences
354 were determined by Welch's t-test (A and B) and one-way ANOVA and the Tukey post hoc test
355 (D, H, I, and J). $p < 0.0001$ (****), $p < 0.001$ (***), $p < 0.01$ (**), and $p < 0.05$ (*).
356
357 **Wall teichoic acid alterations contribute to USA300 sensitivity to cefuroxime in SWF.**

358 Next, we sought to evaluate changes in WTA, which plays a role in the coordination of
359 peptidoglycan synthesis and β-lactam resistance (56, 57). First, we sought to test *tarO,* which
360 encodes a *N*-acetylglucosamine-1-phosphate transferase, the first committed step in WTA
361 production (58). A *tarO* knockout is not within the NTML, and thus was not tested in our screen.
362 A CMRSA10Δ*tarO* was ≥256-fold more susceptible to cefuroxime in MHB but only ~4-fold
363 more susceptible to the β-lactam in SWF relative to the wildtype (Fig. 3C), mirroring the
364 phenotype of the primary determinants identified above (Fig. 2C). We then used targocil, an
365 inhibitor of the WTA flippase TarG **(59)**, to determine if culturing in SWF disrupts TarO or WTA
366 biosynthesis. While targocil is lethal, knocking out genes encoding early steps in the WTA
367 synthesis pathway (*tarO* and *tarA*) or inhibiting their products, which completely block WTA
368 biosynthesis, antagonizes targocil **(60)**. We observed an ~8-fold increase in targocil MIC against
369 wildtype USA300 when tested in SWF relative to MHB, raising the MIC up to 32 μg/mL (Fig.
370 3C). In comparison, the targocil MIC against the Δ*tarO* mutant was >64 μg/mL in both media
371 (Fig. 3C), which together suggests that WTA biosynthesis is at least partially disrupted in SWF.
372 TarO inhibition has been associated with the delocalization of PBP2, leading to increased
373 β-lactam sensitivity **(61)**. Epicatechin gallate (ECg) induces partial delocalization of PBP2 from
374 the division septum, mimicking the effects of TarO inhibition **(61)**. As expected, ECg synergized
375 with cefuroxime against the wild-type USA300 in MHB (FICI = 0.023 ± 0.005; Fig. 3D).
376 However, such synergy was lost when we tested the same combination in SWF (FICI = 2.2 ±
377 0.2; Fig. 3D), suggesting PBP2 was already delocalized, potentially due to WTA biosynthesis
378 disruption, under the wound-like condition.
379 Next, we directly evaluated the abundance of WTA in SWF and MHB (Fig. 3E-G,
380 Supplementary Fig. 10A). We tested both the wild-type USA300 strain and the *tcaA*::Tn mutant

381 identified from the screen (Fig. 2), as *tcaA* encodes a teicoplanin resistance-associated protein
382 involved in WTA retention and robustness of *S. aureus* peptidoglycan crosslinking **(45)**. USA300
383 cultured in SWF showed a significant decrease in WTA abundance relative to MHB (Fig. 3E, F).
384 The WTA abundance of the wild-type grown in SWF was comparable to that observed in the
385 *tcaA*::Tn mutant cultured in MHB or SWF (Fig. 3E; no significant difference across these three
386 conditions). Notably, the WTA bands from the wild-type cultured in SWF migrated slightly
387 further on the PAGE relative to those from an MHB culture (Fig. 3F, G), suggesting a shorter
388 WTA polymer. However, the shorter polymer length was not associated with TcaA, as the same
389 occurred in the *tcaA*::Tn mutant (Fig. 3F, G).

390 WTA, its influence on PBP localization, and gene products associated with that polymer,
391 such as FmtA (a teichoic acid D-Ala esterase) and TcaA, are involved in the structural integrity
392 of the cell envelope, which can alter the bacterial autolysis **(45, 46, 62)**. Therefore, we assessed
393 the 0.02% Triton X-100-induced lysis of USA300, relative to knockouts of *fmtA* and *tcaA,* in
394 MHB and SWF. Wild-type USA300 cells harvested from SWF cultures showed significantly
395 faster Triton-induced lysis rates relative to those from MHB cultures (Fig. 3H, I, Supplementary
396 Fig. 10B-D). There was no further increase in lysis rates in SWF due to disrupting *tcaA* and
397 *fmtA,* where both mutants showed no statistical difference in lysis rate compared to the wild-type
398 cultured in SWF (Fig. 3H, I, Supplementary Fig. 10B-D), suggesting WTA-associated gene
399 products may have already been disrupted in SWF. In all cases, these observations are consistent
400 with the alterations in WTA and PBP localization observed in SWF.

401 Next, we indirectly assessed cell surface charge, which is partly influenced by WTA
402 retention, by quantifying binding to cytochrome c, a highly positively charged protein. A
403 decreased abundance of WTA, a polyribitol phosphate polymer that generally imparts a strong

404 negative charge to the surface **(63)**, should reduce the overall net negative charge of the cell
405 surface. USA300 cultured in SWF showed a significant decrease in binding to cytochrome c
406 compared with MHB (Fig. 3J). We observed a decrease in relative cytochrome c binding to
407 *tcaA*::Tn compared to that of USA300, but no difference in cytochrome c binding between
408 *tcaA*::Tn cultured in MHB and SWF (Fig. 3J). These results align with the respective relative
409 WTA abundance (Fig. 3E). Of note, other factors can also influence surface charge, such as
410 MprF, a phosphatidylglycerol lysyltransferase, which decreases the net negative charge of the
411 cell surface through lysyl modification of the cytoplasmic membrane, conferring resistance to
412 cationic antimicrobials **(64)**. While the cytochrome c binding of *mprF::Tn* in SWF relative to
413 MHB followed the same trend observed for the wild-type strain, the lack of such modification in
414 *mprF*::Tn increased the binding to cytochrome c relative to wild-type USA300 in each of the
415 tested media, as expected (Fig. 3J). Taken together, the results in this section demonstrate WTA-
416 related alterations that may contribute to the increased β-lactam susceptibility of the MRSA
417 USA300 in the wound-mimetic medium.
418
419 **A lack of antibiotic-mediated induction of the GraXSR VraFG system in SWF.**
420 GraXSR VraFG is a five-component system that regulates the bacterial response to cell
421 envelope stress, such as exposure to cationic antimicrobial peptides, through processes that
422 include the DltABCD-mediated D-alanylation of teichoic acids and the MprF-dependent
423 lysylination of phosphatidylglycerol (65). Notably, disruptions of GraR sensitize MRSA to β-
424 lactams (60). *mprF* is positively regulated by GraXSR, and the system is strongly induced by
425 colistin, a cationic antimicrobial peptide **(60)**. Hence, we assessed the colistin-mediated
426 induction of the GraXSR VraFG system in SWF compared to tryptic soy broth (TSB), a standard

427 culture medium, by monitoring luciferase reporter expression under the control of the *mprF*
428 promoter. As previously reported **(60)**, we observed a colistin-mediated *graR*-dependent
429 induction of the *mprF* promoter in TSB, where there was a significant increase in luciferase
430 signal in the presence of colistin in the wild-type (Fig. 4A) but not in the Δ*graR* mutant
431 (Supplementary Fig. 11A-C). Such colistin-mediated *mprF* promoter induction was not observed
432 in SWF (Fig. 4A); instead, a significant *graR*-independent repression of the *mprF* promoter at 3
433 hours by colistin was observed in both the wild-type (Fig. 4A) and the Δ*graR* mutant
434 (Supplementary Fig. 11D-F). To further assess the role of the GraXSR VraFG system in
435 antibiotic response in SWF, we used MAC-545496, a GraR inhibitor previously shown to
436 synergize with β-lactams in MHB **(60)**. As expected, we observed a *graR*-dependent synergy
437 between MAC-545496 and cefuroxime against USA300 in MHB (FICI = 0.036 ± 0.014; Fig.
438 4B; not observed against *graR*::Tn, FICI = 1.04 ± 0.47; Supplementary Fig. 12). Such synergy
439 was lost in SWF (FICI = 2.0 ± 0.0; Fig. 4B). Together, the lack of *mprF* promoter induction by
440 colistin and loss of MAC-545496-cefuroxime synergy in SWF illustrate the lack of stress-
441 mediated induction of GraR and its regulon, and hence the disruption of the GraXSR VraFG cell
442 envelope stress response system, in the simulated wound fluid.

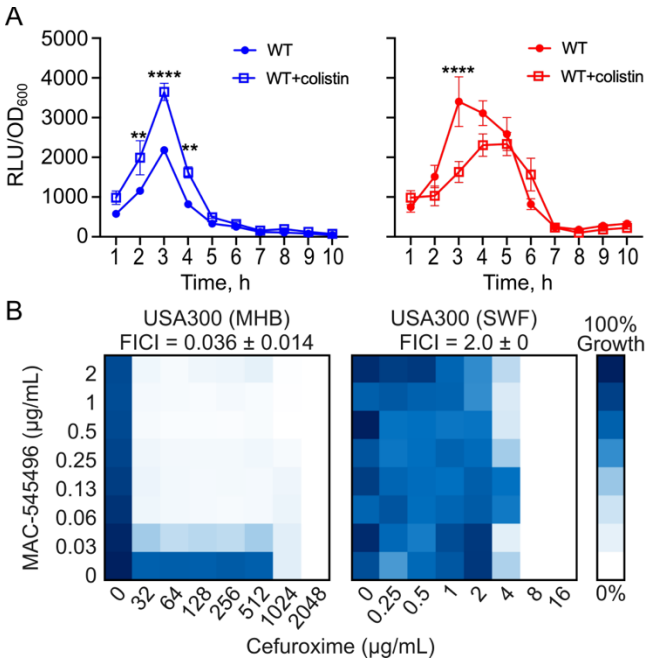

Fig. 4 | Disruption of GraXSR VraFG in SWF contributes to cefuroxime sensitivity. A) Monitoring the luciferase expression under the control of the *mprF* promoter in USA300 over 10 h in TSB (Blue) or SWF (Red) in the presence or absence of 1/32 MIC of colistin. n = 4 shown as mean ± SEM. Significant differences were determined between the with and without colistin conditions by two-way ANOVA and the Bonferroni post hoc test. $p < 0.0001$ (****), $p < 0.001$ (***), $p < 0.01$ (**), $p < 0.05$ (*). B) Representative cefuroxime and MAC-545496 checkerboard assays against *S. aureus* USA300. Dark blue represents high cell density, measured by OD_{600}, n = 3, FICI shown as mean ± SEM.

Ultrastructural, biochemical, and mechanical changes to USA300 grown in SWF.

Next, we further assessed the cell and its envelope using atomic force microscopy (AFM) to compare cell size, surface topography, roughness, elasticity, and adhesion. We observed a significant increase in cell size (height and diameter) and surface roughness of USA300 cultured in SWF relative to that cultured in MHB (Fig. 5A-H, Supplementary Fig. 13, 14). The surface of USA300 cells harvested from SWF culture was more compliant relative to those from MHB,

459 requiring less force to deform (Fig. 5I). Adhesion values between the negatively charged silicon
460 nitride AFM tip and the cell surface were greater for USA300 cells cultured in SWF relative to
461 MHB (Fig. 5J), consistent with the cytochrome c binding assays showing that USA300 cultured
462 in SWF are less negative than those in MHB (Fig. 3J). Together, these results provide further
463 evidence for cell envelope-related alterations in synthetic wound fluid, which underpins the
464 increased β-lactam susceptibility.
465

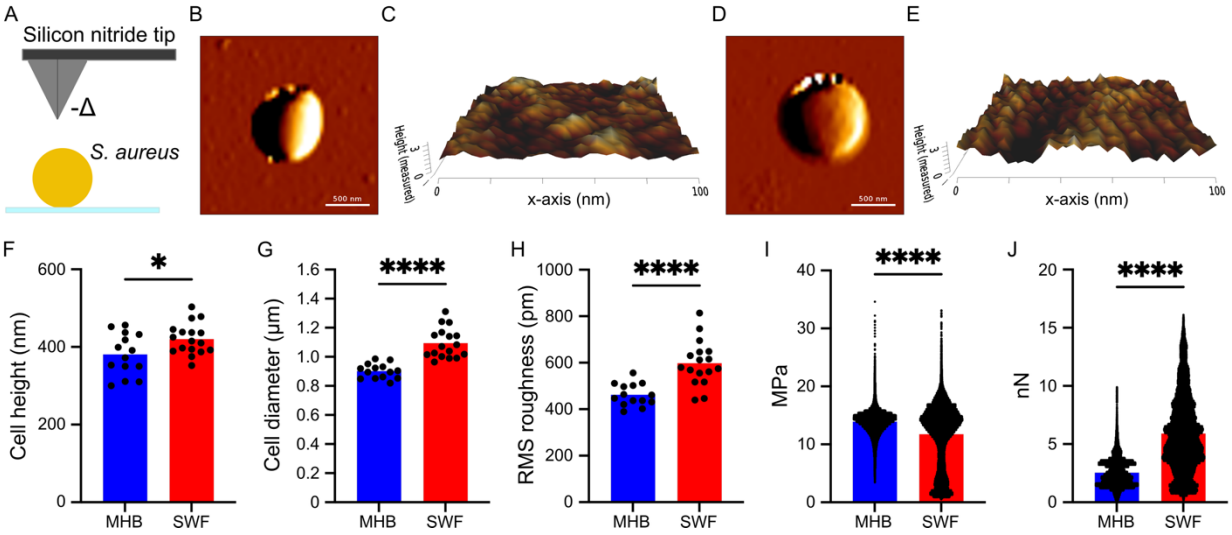

466

467 **Fig. 5 | Atomic force microscopy of USA300 cultured in MHB and SWF**

468 A) A schematic diagram of the AFM probe, B-E) Representative images (B, D) and 3D images of
469 cell surface topography (C, E) of USA300 cultured in MHB (B, C) and SWF (D, E). All AFM
470 images used for quantitative analyses are shown in Supplementary Fig. 13 and 14. F) Cell height
471 of USA300 cultured in MHB and SWF. G) Cell diameter of USA300 cultured in MHB and SWF.
472 H) Root mean squared (RMS) roughness of the flattest 100 nm x 100 nm region from a 0.4 x 0.4
473 µm scan area. I-J) Viscoelasticity and adhesion of USA300 cultured in MHB n = 91079 and
474 SWF n = 118114. Significant differences between USA300 cultured in MHB and SWF were
475 determined by Welch's t-test. $p < 0.0001$ (****), $p < 0.001$ (***), $p < 0.01$ (**), $p < 0.05$ (*).

476

477 **Cefuroxime rescues USA300-infected Galleria larvae.**

478 Next, we sought to determine the efficacy of cefuroxime against USA300 in an *in vivo G.*
479 *mellonella* incision wound infection model. Infection with wild-type USA300 treated with the
480 vehicle control (Glaxal^{TM} base non-medicated cream), led to only 10% and 2.5% larval survival
481 by days 3 and 6 post-infection, respectively (Fig.6). In contrast, a single dose cefuroxime
482 treatment (4 μL of 40% w/w cream, i.e., 1.6 mg/incision) significantly increased the survival of
483 USA300-infected larvae to ~75% and 45% at the same timepoints post-infection ($p<0.0001$; Fig.
484 6). Together, the efficacy of cefuroxime against USA300 *in vivo* aligns with the *in vitro*
485 susceptibility to that β-lactam antibiotic in SWF, demonstrating that this wound exudate-mimetic
486 medium may be superior to MHB for predicting clinical outcomes of MRSA wound infections.

487

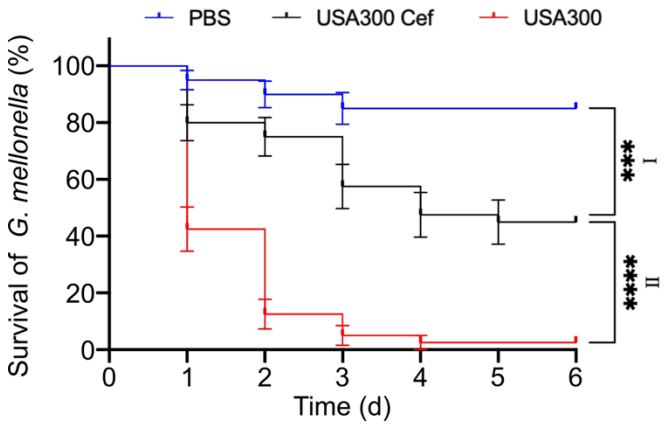

488

489 **Fig. 6 | Cefuroxime increases larval survival *in vivo Galleria* wound infection.**
490 Kaplan-Meier survival curve of larvae shown as mean ± SE. PBS with vehicle treatment (blue),
491 infection with USA300 and vehicle treatment (red), and infection with USA300 and cefuroxime
492 treatment (black), n = 40 from 4 independent experiments. Significant differences were
493 determined between (I; PBS and USA300 Cef) and (II; USA300 and USA300 Cef) by the
494 Logrank (Mantel-Cox) test. $p<0.0001$ (****), $p<0.001$ (***), $p<0.01$ (**), $p<0.05$ (*).

495

496 **Discussion**

497 Standard MHB-based AST assays have been widely used worldwide to guide
498 antimicrobial therapy and study antimicrobial resistance. However, MHB does not accurately
499 reflect the conditions at the site of infection **(66)**, and the clinical outcome often does not
500 correlate with standard AST results (19-21). Further, antibiotic discovery has traditionally relied
501 on standard AST conditions, partly because of regulatory requirements to demonstrate efficacy
502 under such conditions for approval (67), which has likely limited the suite of potential
503 antimicrobial targets and bioactives. Therefore, there are emerging efforts to study bacterial
504 responses and screen for new antimicrobials under infection-relevant conditions to bridge the gap
505 between *in vitro* testing and *in vivo* outcomes [E.g., (45, 68-72)]. Herein, we studied the
506 antibiotic responses of MRSA under wound-infection-mimetic conditions, revealing ~67%
507 discordance in AST results between simulated wound fluid and MHB. Similar discordances were
508 observed in analyses using serum-containing and other eukaryotic cell culture media (e.g.,
509 RPMI) (73, 74). We then sought to elucidate the mechanisms underlying the two most significant
510 antibiotic susceptibility alterations in the MRSA USA300 strain in terms of fold-shift and
511 potential clinical relevance, the unexpected resistance to tetracyclines and sensitization to β-
512 lactams in SWF.

513 We revealed that the unexpected increase in resistance to first-, second-, and third-
514 generation tetracyclines under wound-like conditions is mediated by MntC (Fig. 7A). MntC has
515 not been previously known to confer tetracycline resistance, a role overlooked in standard culture
516 conditions but detected in SWF. We observed an upregulation of *mntC* in SWF relative to MHB,
517 independent of tetracycline exposure, suggesting MntC expression is induced by the culture
518 condition rather than the antibiotic. Interestingly, the observed unexpected resistance to

519 tetracyclines appears to corroborate reports of therapeutic failures with tigecycline (a tetracycline
520 derivative) in soft-tissue, bloodstream, and other infections despite predicted efficacy (75, 76).
521 Also, the upregulation of *mntC*, which is highly conserved among *S. aureus*, in the serum-based
522 SWF aligns with observations from *in vivo* studies and patient samples (77-80). MntC was only
523 expressed *in vivo* or in the presence of serum, and rapidly upregulated in *S. aureus* murine
524 infection (77, 78). Anti-MntC antibodies protected against *S. aureus* in an infant rat model, and
525 MntC could induce a protective immune response; hence, it was identified as a potential vaccine
526 target (77, 78). *mntC* (also referred to as *sitA*) had increased transcription in three healthy
527 persistently colonized volunteers relative to *in vitro* conditions (79) and ranked among the first
528 quartile of upregulated genes in pediatric skin and soft tissue infection (SSTI) and murine SSTI
529 abscesses (80). As such, unexpected clinical failures of tetracyclines against MRSA may occur
530 due to MntC overexpression *in vivo*. These observations, along with the increased survival of
531 *mntC*::Tn-wound infected Galleria larvae, relative to wild-type, upon treatment with doxycycline
532 (Fig. 1G), support that MntC could serve as an *in vivo*, clinically relevant drug target for new
533 antibiotic adjuvants for tetracyclines. Interestingly, infection with an *mntC* knockout increased
534 animal survival in a murine sepsis model, which was attributed to an increased susceptibility of
535 the mutant to oxidative stress **(81)**, aligning with the increased larval survival at day 1 post-
536 infection with *mntC*::Tn relative to USA300 without treatment (Fig. 1G). These observations
537 suggest that MntC may also serve as a target for stand-alone anti-virulence therapy.

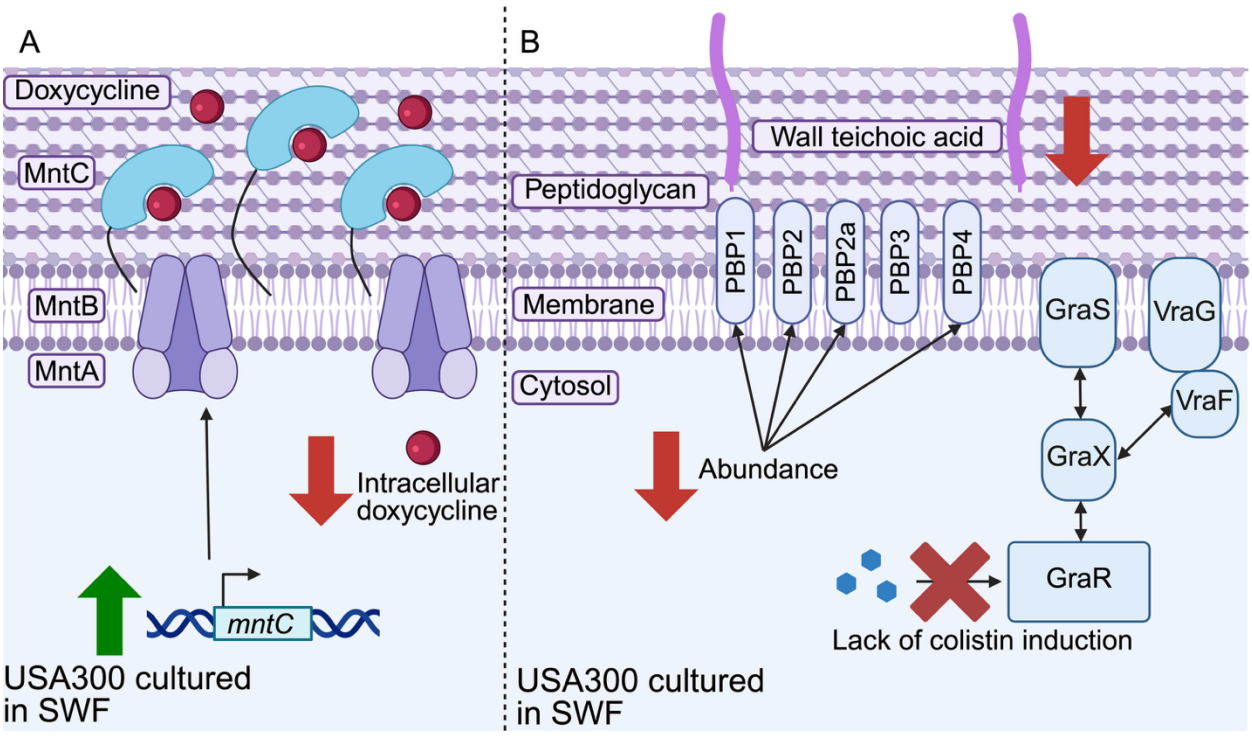

Fig. 7 | Summary of mechanisms underlying the altered susceptibility of MRSA USA300 to tetracyclines and β-lactams under wound infection-like conditions.

A) Summary of alterations in USA300 that led to increased resistance to tetracyclines when cultured in SWF, depicting an increase in expression of MntC, which binds to doxycycline (a tetracycline), reducing its intracellular concentration. B) Summary of cell envelope-related remodelling in USA300 that increased susceptibility to β-lactams when cultured in SWF, displaying decreased abundance of penicillin binding proteins PBP1, 2, 2a, 4 and wall teichoic acid, along with a lack of the antimicrobial peptide colistin-mediated GraXSR VraFG induction. Created using Biorender.

MRSA are characterized by their resistance to β-lactam antibiotics. As such, the significant sensitization of tested MRSA strains from widely circulating lineages to representative β-lactams in the simulated wound fluid is counterintuitive but suggests that β-

552 lactams may be a viable therapy for MRSA wound infections. *In vivo* results from the Galleria
553 incision wound infection model aligned with the *in vitro* data, whereby the β-lactam cefuroxime
554 improved the survival of MRSA USA300-infected larvae (Fig. 6). Interestingly, an observational
555 study of 2096 pediatric skin and soft tissue infection patients at a community-acquired MRSA-
556 endemic region in Philadelphia reported a therapeutic success of empiric β-lactam monotherapy
557 comparable or even superior to that of MRSA-active antibiotics (82), suggesting that β-lactams
558 likely cleared at least some MRSA infections, a regimen that standard AST would have
559 contraindicated. Further, other recent reports have shown that adding β-lactams to the empirical
560 therapy regimen improved bacterial clearance in MRSA bacteremia **(83-86)**. Mechanistically, we
561 revealed that cell envelope remodelling of the MRSA USA300 under wound-like conditions,
562 involving a decreased abundance of penicillin binding proteins PBP1, 2, 2a, 4 and wall teichoic
563 acid, along with a lack of antibiotic-mediated GraXSR VraFG induction (Fig. 7B), underpins the
564 sensitivity of MRSA to β-lactams in SWF. Notably, various cell envelope changes were
565 previously reported for *S. aureus* cultured in serum-containing media, altering responses to cell
566 wall-targeting and membrane-active antibiotics (45, 68). Together, our results and previous
567 observations suggest that MHB-based AST may erroneously exclude β-lactams from therapeutic
568 regimens, and that the wound exudate-like medium may be better than MHB at predicting β-
569 lactam antibiotic efficacy. β-lactams are broad-spectrum, well-tolerated antibiotics that offer oral
570 options **(87)**; hence, accurately predicting their potency and recommending their use when
571 possible would be valuable in the clinic.

572 Overall, host-mimetic media, such as SWF, may better predict bacterial resistance and
573 correlate more closely with positive clinical outcomes. Uncovering antimicrobial susceptibility
574 profiles discordant between infection-relevant (e.g., SWF) and standard (e.g., MHB) culture

575 media may enhance our understanding of antibiotic therapeutic responses during infection. By
576 revealing the mechanisms underlying the discordant phenotypes, we identified MntC as a
577 potential target for new antimicrobials that may reverse resistance to currently available
578 tetracycline antibiotics or suppress virulence *in vivo*. The phenotypes uncovered herein provide
579 an *in vitro* screening platform in SWF for therapeutics targeting MntC. Our AST results in the
580 wound-like medium could also guide and optimize the use of currently available antibiotics.
581

582 **Materials and methods:**

583 **Strains and reagents.** Supplementary Table 1 lists the strains and plasmids, and
584 Supplementary Table 2 lists the primers used in this study. Bacteria were grown in cation-
585 adjusted Mueller-Hinton broth (MHB) or synthetic wound fluid (50% Fetal bovine serum from
586 Fisher Scientific, 50% Maximum recovery diluent (MRD; 1g/L peptone, 8.5g/L NaCl) at 37 ºC,
587 unless otherwise specified.

588

589 **Antimicrobial Susceptibility Testing (AST).** MICs were determined by broth
590 microdilution according to CLSI guidelines **(88)**. The assays were conducted in microtiter plates
591 with a final inoculum adjusted to an OD_{600} of 0.001, prepared by the colony resuspension
592 method. The plates were then incubated at 37ºC with shaking, and bacterial growth was
593 determined by measuring the OD_{600} after 24 h. When MIC values were not reached within the
594 tested concentration range, the highest tested concentration was considered half the MIC. The
595 fractional inhibitory concentration indices (FICI) were calculated as FICI = (MIC_A in
596 combination/MIC_A alone) + (MIC_B in combination/MIC_B alone). FICI values ≤0.5 were
597 interpreted as synergy, >0.5 to ≤4.0 as additive or indifferent, and >4.0 as antagonistic.

598

599 **Nebraska transposon mutant library (NTML) screen.** Overnight cultures of the
600 NTML **(40)** were prepared in 384-well plates using Biomatrix BM6-BC (S&P Robotics Inc.) in
601 MHB with 5 µg/mL erythromycin (Sigma-Aldrich). The following day, these overnight cultures
602 were used to inoculate MHB or SWF with or without doxycycline (Fisher Scientific) or
603 cefuroxime (Sigma-Aldrich), at the concentrations indicated in the results section, using the
604 BM6-BC. All 384-well plates were incubated at 37 ºC and 600 RPM, and the OD_{600} was read
605 after 24 h.

606

607 **Dose-response assay.** Selected NTML strains were re-arrayed and inoculated into 96-
608 well plates in MHB containing 5 µg/mL erythromycin using the BM6-BC. The following day,
609 96-well plates with varying antibiotic concentrations in MHB and SWF were inoculated using
610 the BM6-BC. All plates were incubated at 37 ºC and 600 RPM, and the OD_{600} was read after 24
611 h.

612

613 **Genetic complementation.** To complement *mntB*::Tn and *mntC*::Tn, PCR fragments
614 were amplified using USA300 gDNA as template and primer pairs (listed in Supplementary
615 Table 2): mntB_compF3_AvrII and mntB_compR2_BamHI for *mntB*, mntB_compF3_AvrII and
616 mntC_compR_BamHI for *mntBC*, and mntC_compF3_AvrII and mntC_compR_BamHI for
617 *mntC*. Fragments and pKK22-Pfba were digested with AvrII and BamHI (New England Biolabs),
618 and the plasmid was alkaline phosphatase-treated (using Antarctic phosphatase, New England
619 Biolabs), followed by ligation with T4 DNA ligase (New England Biolabs) to generate the
620 complementation vectors, pKK22-Pfba-*mntB*, pKK22-Pfba-*mntBC*, and pKK22-Pfba-*mntC*.
621 Complementation and control vectors were transformed into electrocompetent *S. aureus* strains
622 by electroporation (Bio-Rad) (89).

623

624 **Doxycycline accumulation assay.** Cultures were started from a single colony and
625 incubated overnight in MHB or SWF at 37 ºC with shaking, then sub-cultured by diluting to an
626 OD_{600} of 0.1 in fresh media and further incubated for 6 h. Cells were harvested from the sub-
627 cultures and resuspended at an OD_{600} of 1 in MHB or SWF. Doxycycline was added to 1 mL of
628 these OD-adjusted cultures at a final concentration of 5 µg/mL, and the cultures were incubated

629 for 30 min at 37 ºC. Cells were pelleted, resuspended in 1 mL of fresh culture media, and
630 incubated for 15 min at 37 ºC. The cells were then washed twice with PBS and resuspended in
631 0.5 mL of PBS, followed by dispensing of 100 µL aliquots into 96-well black plates in triplicate
632 and read at λ_{ex} = 400 nm / λ_{em} = 530 nm. The bacterial suspensions were also transferred to a
633 clear 96-well plate for OD_{600} measurement. All centrifugation steps were at 6,000 × g for 1 min.
634
635 **Protein overexpression and purification.** *mntC* was cloned into pET28a(+) and
636 transformed into $CaCl_2$ chemically competent *E. coli* BL21 by heat shock. Bacterial cultures
637 were incubated at 30 ºC and 250 RPM until an OD_{600} of ~0.8 was reached, then induced with 0.5
638 mM IPTG and further incubated for 5 h at 30 ºC. Cells were harvested, resuspended in lysis
639 buffer [50 mM sodium phosphate, 500 mM NaCl, cOmplete™ protease inhibitor cocktail
640 (Roche), pH 8.0], and lysed using Lysing Matrix B (MP Biomedicals) and the FastPrep-24™.
641 The supernatants were separated from the insoluble fractions by centrifugation at 10,000 × g for
642 15 min at 4 ºC. His-tagged proteins were batch purified from the supernatants using His-select
643 nickel-affinity gel (Sigma-Aldrich), washed three times with wash buffer (50 mM sodium
644 phosphate, 500 mM NaCl, 5 mM imidazole, pH 8.0), and eluted with elution buffer (50 mM
645 sodium phosphate, 500 mM NaCl, 250 mM imidazole, pH 8.0), followed by detection on a 12%
646 acrylamide gel (Bio-Rad) stained with PageBlue™ (Fisher Scientific). The eluted protein was
647 dialyzed using 10 kDa SnakeSkin™ dialysis tubing (Fisher Scientific) into 20 mM HEPES, pH
648 7.4, 100 mM NaCl buffer, then quantified using the Bradford method with protein assay dye
649 reagent concentrate (Bio-Rad).
650

651 **Doxycycline binding assay.** Purified MntC, bovine serum albumin (BSA), and lysozyme
652 solutions in dialysis buffer (20 mM HEPES, pH 7.4, 100 mM NaCl) were each incubated at 37
653 ºC with doxycycline in the dark for 4 h at a final volume of 200 µL and final concentration of 32
654 µM of protein and 16 µM of doxycycline in 96-well black plates. Wells containing only 200 µL
655 of buffer with 16 µM of doxycycline and 200 µL of buffer with 32 µM of protein were used for
656 background subtraction of fluorescent signal. Plates were then read at λ_{ex} = 390 nm / λ_{em} = 550
657 nm.
658
659 **RNA extraction.** USA300 cultures were grown overnight and diluted to an OD_{600} of 0.05
660 in MHB or SWF. Cells were grown at 37 ºC to an OD_{600} of 0.6, then treated with doxycycline (8
661 µg/mL) or vehicle control (ultrapure water) for 30 minutes. Aliquots (6 mL) of the cultures were
662 collected, centrifuged at 3,320 × g for 10 min. RNA was extracted using Monarch Total RNA
663 miniprep (New England Biolabs), followed by treatment with Invitrogen Turbo DNA-free DNase
664 (Fisher Scientific) following the manufacturer's protocol. RNA purity was assessed by
665 measuring the ratio of absorbance at 260 nm to 280 nm (values obtained ~2.0).
666
667 **cDNA synthesis and RT-PCR.** RNA was converted to cDNA with Superscript™ III
668 First-Strand Synthesis System (Fisher Scientific) following the manufacturer's protocol. RT-PCR
669 was performed using the QuantStudio™ 5 Real-Time PCR (Thermo Fisher Scientific) with
670 FastStart SYBR Green (Roche). Fold change in gene expression was calculated using the Pfaffl
671 Method **(90)** relative to *arcC* and 16s rRNA.
672

673 ***Galleria mellonella* incision wound infection model.** *G. mellonella* larvae weighing
674 ~300 mg were selected, anesthetized by chilling at 4 ºC for 10 minutes, and kept on ice during
675 incision and treatment application. Incisions spanning the third segment from the posterior end of
676 the larvae were made parasagittally on the dorsal side. Larvae were inoculated with 2 µL of
677 inoculum (0.0001 OD_{600}/mg of larva weight). After 30 min, 4 µL of a 10% w/w doxycycline
678 compounded in Glaxal™ Base, 40% w/w cefuroxime compounded in Glaxal™ Base, or vehicle
679 control (water in Glaxal™ Base) was applied to the inoculated wounds. Worms were then
680 incubated at 37 ºC and monitored for survival for 6 days.
681
682 **Lysis Assay.** Overnight cultures were diluted to an OD_{600} of 0.1 and grown to an OD_{600} of
683 0.8. Cells were washed and resuspended in PBS or PBS containing 0.02% Triton X-100 (Fisher
684 Scientific) at a cell density of 1 OD/mL. The bacterial suspensions were dispensed into 200 µL
685 aliquots in triplicate in 96-well plates, incubated at 37 ºC with shaking in the plate reader, and
686 their OD_{600} was read every 15 min for 6 h.
687
688 **Cytochrome c binding assay.** The assay was performed as previously described **(91)**.
689 Briefly, overnight cultures were adjusted to an OD_{600} of 1, and 8 mL were pelleted, washed twice
690 in MOPS buffer (20 mM, pH 7.0), and resuspended in a total volume of 200 µL MOPS. A 50 µL
691 aliquot of a 2.5 mg/mL cytochrome c solution (Sigma-Aldrich) was added to the 200 µL
692 resuspended culture and incubated at room temperature for 10 min. The samples were then
693 pelleted at 16,000 × g for 1 min, and 200 µL of the supernatants were dispensed into 96-well
694 plates, and their absorbance was read at 530 nm (A_{530nm}). *mprF*::Tn was used as a positive
695 control.

696

697 **Bioluminescence assay.** The luciferase expression assay was conducted as previously
698 described **(60)**, except that bacteria were cultured in either TSB or SWF.

699

700 **WTA isolation.** Crude WTA was isolated as previously described **(92)**, with minor
701 modifications to normalize the quantity of bacteria prior to WTA isolation. Briefly, overnight
702 cultures in either MHB or SWF were washed once with buffer 1 (50 mM MES, pH 6.5) and
703 volumes corresponding to an OD_{600} of 5 were centrifuged at 5,000 × g, resuspended in buffer 2
704 [4% (w/v) SDS, 50 mM MES, pH 6.5], and boiled for 1 h, followed by washing in buffer 1 and
705 transferring into 1.5 mL microcentrifuge tubes. Pellets were then washed with 1.4 mL of buffer
706 2, then with 1.4 mL of buffer 3 (2% NaCl, 50 mM MES, pH 6.5), followed by 1.4 mL of buffer 1
707 with all spins at 16,000 × g for 1 min. Pellets were resuspended in 1 mL of digestion buffer [20
708 mM Tris-HCl, pH 8.0, 0.5% (w/v) SDS] with the addition of 10 µL of 2 mg/mL proteinase K.
709 Samples were digested at 50 ºC for 4 h with shaking (1000 rpm). Pellets were then washed with
710 1.4 mL of buffer 3, followed by three 1.4 mL washes of ultrapure water. The pellets were then
711 resuspended in 1 mL of 0.1 M NaOH and incubated at 20 ºC for 16 h at 1000 rpm. The samples
712 were then centrifuged at 16,000 × g for 1 min, and 750 µL of the supernatants were transferred to
713 a new microcentrifuge tube. Subsequently, 250 µL of 1 M Tris-HCl, pH 7.8, was added to
714 neutralize the reaction.

715

716 **WTA PAGE.** Aliquots (15 µL) of crude WTA were mixed with 5 µL of 4x loading dye
717 (50% glycerol with bromophenol blue), and 10 µL was loaded and separated on tricine
718 polyacrylamide gels at 40 mA (92) until the dye front had reached the bottom of the gel. Gels

719 were washed three times with ultrapure water, then stained with Alcian Blue 8GX (Fisher
720 Scientific, 1 mg/mL) overnight, and destained with ultrapure water until the bands became
721 visible.
722
723 **Membrane preparation.** Cultures grown overnight at 37 ºC with shaking were diluted to
724 an OD_{600} of 0.05 and then grown to an OD_{600} of 0.8. The cultures were pelleted, resuspended in
725 PBS, and lysed using Lysing Matrix B (MP Biomedicals) and the FastPrep-24™. Cell debris was
726 pelleted at 10,000 × g for 30 min, and the supernatant was centrifuged at 40,000 rpm for 1h to
727 pellet the membrane, which was then resuspended in PBS, and its protein content was quantified
728 by the Bradford method using protein assay dye reagent concentrate (Bio-Rad).
729
730 **BOCILLIN™ FL assay.** Membrane fractions (equivalent to 30 µg of protein content)
731 from USA300 and *pbp4*::Tn cultured in MHB and SWF were incubated with 20 µM of
732 BOCILLIN™ FL (Fisher Scientific) at 37 ºC for 10 min, followed by the addition of 4x Laemmli
733 buffer and boiling for 5 min. Membrane samples were resolved on 10% SDS-PAGE running at
734 80V for 30 min, followed by 120V for 2.25 h. Gels were then visualized using the Typhoon FLA
735 7000 gel scanner (GE Healthcare), and the band intensities were subsequently quantified with
736 ImageJ. PBP quantifications were background-subtracted by membrane-free BOCILLIN™ FL
737 lanes.
738
739 **PBP2a western blot.** Membrane fractions (equivalent to 10 µg of protein content) from
740 USA300 and *pbp2a*::Tn cultured in MHB and SWF were resolved on 10% SDS-PAGE, running
741 at 80 V for 30 min, followed by 120 V for 2.25 h. Protein bands were transferred to

742 nitrocellulose film using a Mini Trans-Blot® Cell (Bio-Rad) at 100 V for 2 h. The nitrocellulose
743 membrane was then blocked overnight at 4 ºC with Blocker™ FL (Thermo Scientific). The
744 primary antibody, mouse anti-*S. aureus*-PBP2a (Thermo Fisher Scientific) (1:1000 dilution in
745 Blocker™ FL), was incubated for 2 h at room temperature with rocking. The secondary antibody,
746 a horseradish peroxidase-conjugated sheep anti-Mouse IgG (Thermo Scientific) (1:1000 dilution
747 in Blocker™ FL buffer), was incubated for 2 h at room temperature with rocking. The blot was
748 developed with 1-Step™ Ultra TMB-Blotting Solution (Thermo Scientific) for 10 min, then
749 visualized on the Gel Doc™ EZ imager (Bio-Rad), and band intensities were subsequently
750 quantified with ImageJ.
751
752 **Atomic force microscopy (AFM) imaging.** AFM (Nanowizard III; JPK Instruments,
753 Berlin, Germany) in quantitative imaging (QI™) mode **(93, 94)** was used to analyze cell surface
754 topography and mechanics of USA300 cells cultured in MHB and SWF. Overnight cultures of
755 USA300 in MHB and SWF were diluted to an OD_{600} of 0.05 and grown to an OD_{600} of 0.6. Cells
756 were then washed three times in PBS and resuspended to an OD_{600} of 0.125 and deposited onto
757 clean, Cell-Tak™ (Corning®)-coated coverslips **(95)**, incubated for 30 min at room temperature
758 followed by rinsing with ultrapure water three times, air dried (30 min) at room temperature, and
759 imaged using non-conductive silicon nitride cantilevers (Multi-cantilever Tip (MLCT), D
760 cantilever, nominal k = 0.03 N/m and tip radius 20 nm; Bruker, USA). Cantilever spring constant
761 (0.028 N/m) was calibrated using the thermal noise method **(96)**. QI™ force curves at each pixel
762 of a 128 × 128 raster scan were collected using a Z-length of 1000 nm, setpoint of 2 nN, and a
763 raster scan of 100 µm/s, along with a subset of force curves within a 0.4 × 0.4 nm square in the

764 center of the cell. Force curves were batch-processed using JPK SPM Data Processing software
765 (version 5.1, JPK, Berlin, Germany), and histogram data were exported to Excel.
766
767 **Statistical analysis.** All statistical analyses were calculated using GraphPad Prism 10. The
768 statistical test used for each assay is indicated in the figure captions.
769
770 **Acknowledgements**:
771
772 This work was funded by a New Frontiers in Research Funds exploration grant (NFRFE-2021-
773 00398), a Saskatchewan Health Research Foundation establishment grant (6115), a Canadian
774 Institutes of Health Research grant (202403PPE-522800), and start-up funds from the Faculty of
775 Science at the University of Regina to OME. O.M.E. holds a Canada Research Chair in
776 Chemogenomics and Antimicrobial Research (CRC-2024-00304). C.D.R. was supported by a
777 Canadian Institutes of Health Research Canada Graduate Scholarship – Master's (CGS-M)
778 award. Work in the T.E.S.D. laboratory was funded by a Natural Sciences and Engineering
779 Research Council of Canada discovery grant.

References

1. R. Laxminarayan *et al.*, Antibiotic resistance-the need for global solutions. *Lancet Infect Dis* **13**, 1057-1098 (2013).
2. C. B. Ibberson, M. Whiteley, The social life of microbes in chronic infection. *Current opinion in microbiology* **53**, 44-50 (2020).
3. G. S. Lazarus *et al.*, Definitions and guidelines for assessment of wounds and evaluation of healing. *Wound Repair Regen* **2**, 165-170 (1994).
4. G. S. Schultz, G. A. Chin, L. Moldawer, R. F. Diegelmann, "Principles of Wound Healing" in Mechanisms of Vascular Disease: A Reference Book for Vascular Specialists, R. Fitridge, M. Thompson, Eds. (Adelaide (AU), 2011).
5. K. F. Cutting, Wound exudate: composition and functions. *Br J Community Nurs* **8**, suppl 4-9 (2003).
6. V. Falanga *et al.*, Chronic wounds. *Nat Rev Dis Primers* **8**, 50 (2022).
7. D. Queen, K. Harding, What's the true costs of wounds faced by different healthcare systems around the world? *International Wound Journal* **20**, 3935-3938 (2023).
8. D. Queen, K. Harding, Estimating the cost of wounds both nationally and regionally within the top 10 highest spenders. *Int Wound J* **21**, e14709 (2024).
9. K. Rahim *et al.*, Bacterial Contribution in Chronicity of Wounds. *Microb Ecol* **73**, 710-721 (2017).
10. C. J. Murray *et al.*, Global burden of bacterial antimicrobial resistance in 2019: a systematic analysis. *The lancet* **399**, 629-655 (2022).
11. S. Y. C. Tong, J. S. Davis, E. Eichenberger, T. L. Holland, V. G. Fowler, *Staphylococcus aureus* Infections: Epidemiology, Pathophysiology, Clinical Manifestations, and Management. *Clinical Microbiology Reviews* **28**, 603-661 (2015).
12. W. Norbury *et al.*, Infection in Burns. *Surg Infect* **17**, 250-255 (2016).
13. K. Gjødsbøl *et al.*, Multiple bacterial species reside in chronic wounds: a longitudinal study. *Int Wound J* **3**, 225-231 (2006).
14. M. Pastagia, L. C. Kleinman, E. G. Lacerda de la Cruz, S. G. Jenkins, Predicting risk for death from MRSA bacteremia. *Emerg Infect Dis* **18**, 1072-1080 (2012).
15. WHO (2017) Prioritization of pathogens to guide discovery, research and development of new antibiotics for drug-resistant bacterial infections including tuberculosis. (World Health Organization, Geneva).
16. K. A. Nichol *et al.*, Characterization of MRSA in Canada from 2007 to 2016. *J Antimicrob Chemother* **74**, iv55-iv63 (2019).
17. J. H. Mueller, J. Hinton, A protein-free medium for primary isolation of the Gonococcus and Meningococcus. *Proc. Soc. Expt. Biol. Med.* **48**, 330-333 (1941).
18. CLSI, *Performance Standards for Antimicrobial Susceptibility Testing; 27th Edition. CLSI supplement M100.* (Clinical and Laboratory Standards Institute, Wayne, PA, 2017).
19. A. P. Macgowan, B. W. P. o. R. Surveillance, Clinical implications of antimicrobial resistance for therapy. *J Antimicrob Chemother* **62 Suppl 2**, ii105-114 (2008).
20. M. N. Hurley, A. H. Ariff, C. Bertenshaw, J. Bhatt, A. R. Smyth, Results of antibiotic susceptibility testing do not influence clinical outcome in children with cystic fibrosis. *J Cyst Fibros* **11**, 288-292 (2012).
21. A. L. Smith, S. B. Fiel, N. Mayer-Hamblett, B. Ramsey, J. L. Burns, Susceptibility testing of *Pseudomonas aeruginosa* isolates and clinical response to parenteral antibiotic administration: lack of association in cystic fibrosis. *Chest* **123**, 1495-1502 (2003).

826 22. M. Tong *et al.*, Gene Dispensability in *Escherichia coli* Grown in Thirty Different Carbon
827 Environments. *mBio* **11** (2020).
828 23. S. Zlitni, L. F. Ferruccio, E. D. Brown, Metabolic suppression identifies new antibacterial
829 inhibitors under nutrient limitation. *Nat Chem Biol* **9**, 796-804 (2013).
830 24. P. G. Bowler, S. A. Jones, M. Walker, D. Parsons, Microbicidal properties of a silver-
831 containing hydrofiber dressing against a variety of burn wound pathogens. *J Burn Care*
832 *Rehabil* **25**, 192-196 (2004).
833 25. Anonymous, Wound exudate and the role of dressings. A consensus document. *Int Wound*
834 *J* **5 Suppl 1**, iii-12 (2008).
835 26. E. Aiba-Kojima *et al.*, Characterization of wound drainage fluids as a source of soluble
836 factors associated with wound healing: comparison with platelet-rich plasma and
837 potential use in cell culture. *Wound Repair Regen* **15**, 511-520 (2007).
838 27. S. Iizaka *et al.*, Do nutritional markers in wound fluid reflect pressure ulcer status?
839 *Wound Repair Regen* **18**, 31-37 (2010).
840 28. T. J. James, M. A. Hughes, G. W. Cherry, R. P. Taylor, Simple biochemical markers to
841 assess chronic wounds. *Wound Repair Regen* **8**, 264-269 (2000).
842 29. N. J. Trengove, S. R. Langton, M. C. Stacey, Biochemical analysis of wound fluid from
843 nonhealing and healing chronic leg ulcers. *Wound Repair Regen* **4**, 234-239 (1996).
844 30. D. Y. Lee *et al.*, Review of the Current Research on Fetal Bovine Serum and the
845 Development of Cultured Meat. *Food Sci Anim Resour* **42**, 775-799 (2022).
846 31. E. A. Slade, R. M. S. Thorn, A. Young, D. M. Reynolds, An *in vitro* collagen perfusion
847 wound biofilm model; with applications for antimicrobial studies and microbial
848 metabolomics. *BMC Microbiol* **19**, 310 (2019).
849 32. A. F. Rowley, N. A. Ratcliffe, A histological study of wound healing and hemocyte
850 function in the wax-moth *Galleria mellonella*. *J Morphol* **157**, 181-199 (1978).
851 33. E. Maslova *et al.*, An Invertebrate Burn Wound Model That Recapitulates the Hallmarks
852 of Burn Trauma and Infection Seen in Mammalian Models. *Front Microbiol* **11**, 998
853 (2020).
854 34. M. L. Nelson, S. B. Levy, The history of the tetracyclines. *Ann Ny Acad Sci* **1241**, 17-32
855 (2011).
856 35. N. M. Brown, A. L. Goodman, C. Horner, A. Jenkins, E. M. Brown, Treatment of
857 methicillin-resistant *Staphylococcus aureus* (MRSA): updated guidelines from the UK.
858 *JAC Antimicrob Resist* **3**, dlaa114 (2021).
859 36. M. A. Farha *et al.*, Inhibition of WTA Synthesis Blocks the Cooperative Action of PBPs
860 and Sensitizes MRSA to beta-Lactams. *Acs Chem Biol* **8**, 226-233 (2013).
861 37. S. Christianson, G. R. Golding, J. Campbell, M. R. Mulvey, Comparative genomics of
862 Canadian epidemic lineages of methicillin-resistant *Staphylococcus aureus*. *J Clin*
863 *Microbiol* **45**, 1904-1911 (2007).
864 38. CLSI, Performance Standards for Antimicrobial Susceptibility Testing CLSI supplement
865 M100. *Approved Standard, Pennsylvania* **33rd ed** (2023).
866 39. CLSI, Performance Standards for Antimicrobial Susceptibility Testing CLSI supplement
867 M100. *Approved Standard, Pennsylvania* **19th ed** (2009).
868 40. P. D. Fey *et al.*, A genetic resource for rapid and comprehensive phenotype screening of
869 nonessential *Staphylococcus aureus* genes. *MBio* **4**, e00537-00512 (2013).

41. M. J. Horsburgh *et al.*, MntR modulates expression of the PerR regulon and superoxide resistance in *Staphylococcus aureus* through control of manganese uptake. *Mol Microbiol* **44**, 1269-1286 (2002).
42. X. Tan, Z. Song, Z. Wang, Characterization of the interaction between bovine serum albumin and doxycycline by chemiluminescence and molecular docking. *Instrumentation Science & Technology* **44**, 294-307 (2016).
43. N. Ramarao, C. Nielsen-Leroux, D. Lereclus, The insect *Galleria mellonella* as a powerful infection model to investigate bacterial pathogenesis. *J Vis Exp* 10.3791/4392, e4392 (2012).
44. J. Glavis-Bloom, M. Muhammed, E. Mylonakis, Of model hosts and man: using *Caenorhabditis elegans*, *Drosophila melanogaster* and *Galleria mellonella* as model hosts for infectious disease research. *Advances in experimental medicine and biology* **710**, 11-17 (2012).
45. E. J. A. Douglas *et al.*, Extensive re-modelling of the cell wall during the development of *Staphylococcus aureus* bacteraemia. *eLife* 10.7554/elife.87026.2 (2023).
46. M. M. Rahman *et al.*, The *Staphylococcus aureus* Methicillin Resistance Factor FmtA Is a d-Amino Esterase That Acts on Teichoic Acids. *mBio* **7**, e02070-02015 (2016).
47. B. J. Hartman, A. Tomasz, Low-affinity penicillin-binding protein associated with beta-lactam resistance in *Staphylococcus aureus*. *J Bacteriol* **158**, 513-516 (1984).
48. P. Reed *et al.*, *Staphylococcus aureus* Survives with a Minimal Peptidoglycan Synthesis Machine but Sacrifices Virulence and Antibiotic Resistance. *PLoS Pathog* **11**, e1004891 (2015).
49. M. Falord, G. Karimova, A. Hiron, T. Msadek, GraXSR Proteins Interact with the VraFG ABC Transporter To Form a Five-Component System Required for Cationic Antimicrobial Peptide Sensing and Resistance in *Staphylococcus aureus*. *Antimicrob Agents Ch* **56**, 1047-1058 (2012).
50. Y.-H. Huang *et al.*, A novel σ^B regulatory module in *Staphylococcus aureus:* Unraveling the multifaceted roles of RsbU domains in stress response mechanisms. *Journal of Microbiology, Immunology and Infection* https://doi.org/10.1016/j.jmii.2025.05.007 (2025).
51. S. Fuchs *et al.*, AureoWiki‐The repository of the *Staphylococcus aureus* research and annotation community. *International Journal of Medical Microbiology* **308**, 558-568 (2018).
52. K. D. Mlynek *et al.*, Effects of Low-Dose Amoxicillin on *Staphylococcus aureus* USA300 Biofilms. *Antimicrob Agents Chemother* **60**, 2639-2651 (2016).
53. J. P. S. Maria *et al.*, Compound-gene interaction mapping reveals distinct roles for *Staphylococcus aureus* teichoic acids. *P Natl Acad Sci USA* **111**, 12510-12515 (2014).
54. A. S. Lee *et al.*, Methicillin-resistant *Staphylococcus aureus*. *Nature Reviews Disease Primers* **4** (2018).
55. S. M. Hamilton *et al.*, High-Level Resistance of *Staphylococcus aureus* to beta-Lactam Antibiotics Mediated by Penicillin-Binding Protein 4 (PBP4). *Antimicrob Agents Chemother* **61** (2017).
56. E. W. C. Sewell, E. D. Brown, Taking aim at wall teichoic acid synthesis: new biology and new leads for antibiotics. *Journal of Antibiotics* **67**, 43-51 (2014).

57. J. Campbell *et al.*, Synthetic Lethal Compound Combinations Reveal a Fundamental Connection between Wall Teichoic Acid and Peptidoglycan Biosyntheses in *Staphylococcus aureus*. *Acs Chemical Biology* **6**, 106-116 (2011).
58. M. A. D'Elia, J. A. Henderson, T. J. Beveridge, D. E. Heinrichs, E. D. Brown, The *N*-Acetylmannosamine Transferase Catalyzes the First Committed Step of Teichoic Acid Assembly in *Bacillus subtilis* and *Staphylococcus aureus*. *J Bacteriol* **191**, 4030-4034 (2009).
59. K. Lee, J. Campbell, J. G. Swoboda, G. D. Cuny, S. Walker, Development of improved inhibitors of wall teichoic acid biosynthesis with potent activity against *Staphylococcus aureus*. *Bioorg Med Chem Lett* **20**, 1767-1770 (2010).
60. O. M. El-Halfawy *et al.*, Discovery of an antivirulence compound that reverses beta-lactam resistance in MRSA. *Nat Chem Biol* **16**, 143-149 (2020).
61. Y. Lu *et al.*, Modulation of MRSA virulence gene expression by the wall teichoic acid enzyme TarO. *Nat Commun* **14**, 1594 (2023).
62. H. Komatsuzawa *et al.*, Cloning and characterization of the *fmt* gene which affects the methicillin resistance level and autolysis in the presence of triton X-100 in methicillin-resistant *Staphylococcus aureus*. *Antimicrob Agents Ch* **41**, 2355-2361 (1997).
63. G. Xia, T. Kohler, A. Peschel, The wall teichoic acid and lipoteichoic acid polymers of *Staphylococcus aureus*. *Int J Med Microbiol* **300**, 148-154 (2010).
64. C. J. Slavetinsky *et al.*, Sensitizing *Staphylococcus aureus* to antibacterial agents by decoding and blocking the lipid flippase MprF. *Elife* **11** (2022).
65. M. Falord, U. Mader, A. Hiron, M. Debarbouille, T. Msadek, Investigation of the *Staphylococcus aureus* GraSR regulon reveals novel links to virulence, stress response and cell wall signal transduction pathways. *PLoS One* **6**, e21323 (2011).
66. M. A. Farha, M. M. Tu, E. D. Brown, Important challenges to finding new leads for new antibiotics. *Current opinion in microbiology* **83** (2025).
67. A. van Belkum *et al.*, Developmental roadmap for antimicrobial susceptibility testing systems. *Nat Rev Microbiol* **17**, 51-62 (2019).
68. E. V. K. Ledger, S. Mesnage, A. M. Edwards, Human serum triggers antibiotic tolerance in *Staphylococcus aureus*. *Nat Commun* **13**, 2041 (2022).
69. G. A. Somerville *et al.*, Human Serum Alters the Metabolism and Antibiotic Susceptibility of *Staphylococcus aureus*. *J Proteome Res* **21**, 1467-1474 (2022).
70. B. Weber *et al.*, Genetic and Chemical Screening in Human Blood Serum Reveals Unique Antibacterial Targets and Compounds against *Klebsiella pneumoniae*. *Cell reports* **32 3**, 107927 (2020).
71. G. Di Bonaventura *et al.*, Repurposing High-Throughput Screening Identifies Unconventional Drugs with Antibacterial and Antibiofilm Activities against *Pseudomonas aeruginosa* under Experimental Conditions Relevant to Cystic Fibrosis. *Microbiol Spectr* **11**, e0035223 (2023).
72. L. A. Carfrae *et al.*, Mimicking the human environment in mice reveals that inhibiting biotin biosynthesis is effective against antibiotic-resistant pathogens. *Nat Microbiol* **5**, 93-101 (2020).
73. S. C. Ersoy *et al.*, Correcting a Fundamental Flaw in the Paradigm for Antimicrobial Susceptibility Testing. *EBioMedicine* **20**, 173-181 (2017).

958 74. D. M. Heithoff *et al.*, Re-evaluation of FDA-approved antibiotics with increased
959 diagnostic accuracy for assessment of antimicrobial resistance. *Cell Rep Med* **4**, 101023
960 (2023).
961 75. S. Jin *et al.*, Clinical and microbiological analysis of risk factors for breakthrough
962 bloodstream infection during Tigecycline Therapy. *Scientific Reports* **15**, 4266 (2025).
963 76. M. Parsonage *et al.*, Breakthrough bacteraemia with a susceptible *Enterococcus faecalis*
964 during tigecycline monotherapy. *J Antimicrob Chemother* **65**, 370-374 (2010).
965 77. A. S. Anderson *et al.*, Development of a multicomponent *Staphylococcus aureus* vaccine
966 designed to counter multiple bacterial virulence factors. *Hum Vaccin Immunother* **8**,
967 1585-1594 (2012).
968 78. A. S. Anderson *et al.*, *Staphylococcus aureus* Manganese Transport Protein C Is a Highly
969 Conserved Cell Surface Protein That Elicits Protective Immunity Against *S. aureus* and
970 *Staphylococcus epidermidis*. *The Journal of Infectious Diseases* **205**, 1688-1696 (2012).
971 79. D. Chaves-Moreno *et al.*, Exploring the transcriptome of *Staphylococcus aureus* in its
972 natural niche. *Sci Rep* **6**, 33174 (2016).
973 80. K. Moffitt, E. Cheung, T. Yeung, C. Stamoulis, R. Malley, Analysis of *Staphylococcus*
974 *aureus* Transcriptome in Pediatric Soft Tissue Abscesses and Comparison to Murine
975 Infections. *Infection and Immunity* **89** (2021).
976 81. L. D. Handke, A. V. Gribenko, Y. Timofeyeva, I. L. Scully, A. S. Anderson, MntC-
977 Dependent Manganese Transport Is Essential for *Staphylococcus aureus* Oxidative Stress
978 Resistance and Virulence. *mSphere* **3** (2018).
979 82. D. J. Elliott, T. E. Zaoutis, A. B. Troxel, A. Loh, R. Keren, Empiric antimicrobial therapy
980 for pediatric skin and soft-tissue infections in the era of methicillin-resistant
981 *Staphylococcus aureus*. *Pediatrics* **123**, e959-966 (2009).
982 83. A. Dhand *et al.*, Use of Antistaphylococcal β-Lactams to Increase Daptomycin Activity in
983 Eradicating Persistent Bacteremia Due to Methicillin-Resistant *Staphylococcus aureus*:
984 Role of Enhanced Daptomycin Binding. *Clinical Infectious Diseases* **53**, 158-163 (2011).
985 84. K. E. Barber, C. E. Ireland, N. Bukavyn, M. J. Rybak, Observation of "seesaw effect"
986 with vancomycin, teicoplanin, daptomycin and ceftaroline in 150 unique MRSA strains.
987 *Infect Dis Ther* **3**, 35-43 (2014).
988 85. A. M. Casapao, D. M. Jacobs, D. R. Bowers, N. D. Beyda, T. J. Dilworth, Early
989 Administration of Adjuvant β-Lactam Therapy in Combination with Vancomycin among
990 Patients with Methicillin-Resistant *Staphylococcus aureus* Bloodstream Infection: A
991 Retrospective, Multicenter Analysis. *Pharmacotherapy* **37**, 1347-1356 (2017).
992 86. J. Truong, J. J. Veillette, S. C. Forland, Outcomes of Vancomycin plus a β-Lactam versus
993 Vancomycin Only for Treatment of Methicillin-Resistant *Staphylococcus aureus*
994 Bacteremia. *Antimicrob Agents Ch* **62** (2018).
995 87. K. Bush, P. A. Bradford, β-Lactams and β-Lactamase Inhibitors: An Overview. *Csh*
996 *Perspect Med* **6** (2016).
997 88. CLSI, Methods for dilution antimicrobial susceptibility tests for bacteria that grow
998 aerobically. *Approved Standard, Pennsylvania*, 19087-11898 (2012).
999 89. M. R. Grosser, A. R. Richardson, Method for Preparation and Electroporation of *S.*
1000 *aureus* and *S. epidermidis*. *Methods Mol Biol* **1373**, 51-57 (2016).
1001 90. M. W. Pfaffl, A new mathematical model for relative quantification in real-time RT-PCR.
1002 *Nucleic Acids Res* **29**, e45 (2001).

1003 91. E. J. A. Douglas *et al.*, Antibacterial activity of novel linear polyamines against
1004 *Staphylococcus aureus*. *Frontiers in Microbiology* **13** (2022).
1005 92. K. Kho, T. C. Meredith, Extraction and Analysis of Bacterial Teichoic Acids. *Bio Protoc*
1006 **8**, e3078 (2018).
1007 93. L. Chopinet, C. Formosa, M. P. Rols, R. E. Duval, E. Dague, Imaging living cells surface
1008 and quantifying its properties at high resolution using AFM in QI™ mode. *Micron* **48**,
1009 26-33 (2013).
1010 94. S. V. Bhat *et al.*, Oxidative stress and metabolic perturbations in *Escherichia coli* exposed
1011 to sublethal levels of 2,4-dichlorophenoxyacetic acid. *Chemosphere* **135**, 453-461 (2015).
1012 95. Z. Shahina *et al.*, "Cellulomics of Live Yeast by Advanced and Correlative Microscopy"
1013 in Laboratory Protocols in Fungal Biology: Current Methods in Fungal Biology.
1014 (Springer, 2022), pp. 159-174.
1015 96. J. Lübbe, M. Temmen, P. Rahe, A. Kühnle, M. Reichling, Determining cantilever stiffness
1016 from thermal noise. *Beilstein J Nanotech* **4**, 227-233 (2013).
1017
1018